LU-TP 21-33
June 2021

COSMOLOGICAL IMPLICATIONS OF A QCD-LIKE COMPOSITE HIGGS MODEL

Hristina Hristova

Department of Astronomy and Theoretical Physics, Lund University

Master thesis supervised by Roman Pasechnik
and co-supervised by António Morais

LUNDS
UNIVERSITET

Abstract

Some of the shortcomings of the Standard Model of particle physics are the "unnatural" value of the mass of the Higgs boson and the fact that the model cannot account for the process of baryogenesis — a mechanism which generates the observed asymmetry between matter and anti-matter in the Universe. The former is related to the fundamental scalar nature of the Higgs boson, connected to quadratic divergences in the mass corrections. The latter is related to the fact that the Standard Model does not accommodate all three Sakharov conditions necessary for baryogenesis to occur. We present an effective UV-complete composite Higgs model built in analogy to Quantum Chromodynamics and confined at higher energy scales of $\mathcal{O}$(TeV). The parameter-space of the model and the particle spectra have been explored and first-order phase transitions are sought for. The purpose is to study whether the gravitational waves produced by such events could be detected by the LISA interferometer as well as other proposed projects such as BBO and DECIGO. Albeit not many, such parameter-space points that feature strong first-order phase transitions did indeed cross the sensitivity curves of all three interferometers. A couple of benchmark points produced a very high signal-to-noise ratio value and one of them is within LISA's sensitivity domain. The thesis demonstrates that such strongly confined theories, going by the name of *technicolor*, may indeed provide potentially observable cosmological consequences worth further exploration.

Populärvetenskaplig sammanfattning

In a wonderful talk [1] given at the The Royal Institution of Great Britain [2], professor David Tong expresses his indignation on the following matter. The model that particle physicists have been working on for more than half a century now, carries this rather unfortunate adjective in front: "standard". There is really nothing standard in the model. It is, in fact, quite extraordinary. It successfully describes the quantum world in just 28 independent parameters and is the most accurately tested theoretical model up to date.

Fortunately for us, this model is not at all complete. It is indeed fortunate as it means that there are still theories to be developed and discoveries to be made. What could be classified as unfortunate is that theory advances over experiments and the validity of some very well-established models cannot be tested since the technology to do so is yet to be explored.

One can make a list of topics which the Standard Model does not accommodate very well. Now, however, we shall concentrate on only a few. One topic that bothers some physicists is the definition of the Higgs boson in the Standard Model. Being introduced as a fundamental scalar, we are forced to very (very!) delicately "tweak" the parameters of the Standard Model in such a way that the Higgs boson restores its experimentally observed mass of 125 GeV. It might be that scientists are worrying a bit too much about it but nevertheless such behaviour is indeed quite peculiar and it makes people wonder.

Another issue with the Standard Model is that it cannot account for the observed matter-antimatter asymmetry in the Universe, as one of the three so-called Sakharov conditions are not realized, namely the early Universe should have experienced a thermal inequilibrium with respect to baryon-number-violating reactions. Such a thermal inequilibrium implies a very abrupt transitions from 1) a Universe filled with zero Higgs vacuum expectation value to 2) a Universe filled with non-zero Higgs vacuum expectation value. However, in the Standard Model, such transitions happen very smoothly and do not provide conditions for an asymmetric Universe.

Scientists have introduced various ideas that could both reproduce the values of the conventional and experimentally tested Standard Model and also make it possible for phenomena such as the one described above to occur. One such bright idea is technicolor. In the present thesis, we both redefine the Higgs sector and introduce a mechanism that generates such abrupt transitions. How would we know if the theory we consider points in the right direction? Earlier, it was mentioned that technology has not yet advanced to probe certain models. Nevertheless, it has advanced tremendously and just enough for us to be able to probe something quite amazing, namely gravitational wave signals from such possible transitions. State-of-the-art interferometers such as LISA and the proposed BBO and DECIGO are designed to do just that. Hopefully, some ten years from now we would have a new and exciting story to tell.

Contents

1 Introduction **1**

2 Building the framework **3**

2.1 Technicolor 3

2.2 Electroweak phase transition 4

2.3 Gravitational waves 7

2.3.1 Equilibrium properties of the plasma 8

2.3.2 Microscopic properties of the plasma 10

2.3.3 Hydrodynamical properties of the plasma 11

2.4 The Linear Sigma Model 12

3 Transformation properties of T-quark fields **13**

3.1 The $SU(2)_{\mathrm{W}} \otimes SU(2)_{\mathrm{TC}}$ group representation 14

3.2 The $U(1)_{\mathrm{Y}} \otimes SU(2)_{\mathrm{TC}}$ group representation 15

3.3 A Technicolor Lagrangian 16

4 QCD-like composite Higgs Model **16**

4.1 Scalar and pseudoscalar T-mesons 17

4.2 Breaking chiral symmetry 18

4.3 Breaking electroweak symmetry 20

4.4 Mass spectrum 22

4.5 Tree-level potential and field-dependent masses 26

5 Results and Discussion **28**

5.1 Gravitational wave signals versus peak frequencies 28

5.2 Benchmark points 33

6 Conclusion **36**

7 Acknowledgements **37**

Appendices **38**

A Electroweak phase transition **38**

B The Hubble Time **40**

C Entries of the field-dependent mass-squared Hessian matrices **42**

D CosmoTransitions **44**

Abbreviations

BBO	Big Bang Observer
CP	Charge-Parity
DECIGO	Deci-hertz Interferometer Gravitational wave Observatory
(EW)PT	(ElectroWeak) Phase Transition
(EW)SB	(ElectroWeak) Symmetry Breaking
F/SOPT	First/Second Order Phase Transition
LISA	Laser Interferometer Space Antenna
QCD	Quantum ChromoDynamics
SM	Standard Model
SNR	Signal-to-Noise Ratio
T-	Techni-
TC	TechniColor
TCLσM	TechniColor Linear Sigma Model
THDM	Two-Higgs-Doublet Model
UV	UltraViolet
VEV	Vacuum Expectation Value

1 Introduction

The latest breakthrough for the Standard Model (SM) came with the detection of a particle with a mass of 125 GeV, associated with the long sought for Higgs boson [3, 4]. The definition of the Higgs sector in the model, however, has raised some questions. The trouble is that the SM is applicable only up to a certain cut-off scale. As reasoned below, the theory cannot provide a dynamical reason for the spontaneous symmetry breaking and explain the small mass of the Higgs boson, connected to the so-called hierarchy problem. A fundamental "theory of everything" would be one in which all observables obtain their values "naturally" in the theory and are stable against imperceptible variations of model parameters [5]. Unfortunately, the SM is susceptible to one rather undesirable fine-tuning. This is a result of the existence of a fundamental scalar in the theory as is the Higgs boson. If we introduce some cut-off scale $\Lambda_{\text{cut-off}}$, then the one-loop mass corrections to the Higgs mass-squared would be quadratically divergent ($\delta m_h^2 \propto \Lambda_{\text{cut-off}}^2$) compared to the well-behaved logarithmic divergences in the case of fermionic fields [6]. If we postulate that a fundamental cut-off scale should be, for example, of $\mathcal{O}(10^{19}$ GeV), corresponding to the Planck energy scale [5, 7], then, if we are to recover the experimentally observed mass of the Higgs boson, the counterterms in the SM should be fine-tuned to one part in 10^{15} [8]. Another problem that might very well be related to this one is the fermion mass hierarchy — why is the top quark so much heavier than the electron? Is the mystery behind the origin of light neutrino masses also somewhat connected?

Evidently, the concerns regarding the completeness of the SM do not end there. Various other peculiarities need their explanations, one of them being the scarcity of antimatter in present days, a problem connected to *baryogenesis*. This matter-antimatter asymmetry is summarised with the following baryon-to-photon ratio

$$\rho = \frac{n_b - n_{\bar{b}}}{n_\gamma} \sim 10^{-9},$$

where n_b, $n_{\bar{b}}$ and n_γ are number densities of baryons, antibaryons and photons, respectively. Albeit very small, this ratio is non-zero. Therefore, the existence of a mechanism or a number of conditions that set the scene for a baryon asymmetry in the early Universe is inevitable. Owing to Sakharov [9], we are equipped with the following starting points:

1. Violation of baryon number (B) conservation;
2. Charge-asymmetry and charge-parity (CP) invariance;
3. Thermal inequilibrium with respect to B-violating reactions, which implies a strong first-order phase transition (FOPT);

The first condition is realized within the SM through the so-called sphaleron transitions [10, 11]. The sphaleron is an unstable, time-independent, finite-energy solution to the

field equations in the electroweak theory of coupled $W^{\pm}$, Z^0 and Higgs bosons. Transitions involving sphalerons are suppressed at zero temperatures but become important as temperature increases. Such processes are associated with a net change in baryon and lepton number and they naturally lead to the idea of electroweak baryogenesis [12, 13]. The second condition is also consistent with the SM and such a CP-violation has been observed in neutral K-meson decays. Unlike the first two conditions, the third one needs a beyond-the-SM mechanism. Such a departure from thermal equilibrium can be realized by imposing a condition that cosmological phase transitions have occurred as *first-order* electroweak phase transitions (FOEWPT). In the realm of the SM, the EWPT is bound to happen as a crossover, a second-order phase transition (SOPT) due to the mass of the Higgs which is now known to be 125 GeV. As has been shown in [14], a finite-temperature (hot) FOPT is not realized for Higgs masses exceeding the mass of the $W^{\pm}$ boson.

An extension to the SM seems not only necessary, but inevitable. There are two promising solutions to the problem of the light Higgs mass. One of them is introducing supersymmetric particles. The second one is introducing *technicolor* (TC) — a new strong sector confined at a high energy scale under a new gauge symmetry. Similarly to Quantum Chromodynamics (QCD), this ultraviolet- (UV) complete theory would contain an analogue of quarks and gluons, often referred to as techniquarks (T-quarks) and technigluons, having the corresponding charge known as TC. Even though neither theory stands on experimental grounds yet, the interest seems to be leaning quite strongly towards the idea of supersymmetry. Nevertheless, it is not at all strange to postulate that there exist particles beyond the reach of our current colliders. After all, to our knowledge, the heaviest fundamental particle is the top quark with a mass of $\mathcal{O}(10^2$ GeV). It is apparent that we are yet to learn what is hidden all the way until the Planck mass.

The following thesis is concerned with a minimal formulation of the composite Higgs model with a simple QCD-like UV completion. Such models have proven useful in many ambitious implementations such as supersymmetric models and grand unification theories [15]. Moreover, they provide a dynamical explanation to the origin of electroweak symmetry breaking (EWSB) without introducing elementary scalars. Instead, the Higgs is represented as a bound state of a new strongly coupled sector [16]. Here, we present a particular scenario of a composite Two-Higgs-Doublet model (THDM) where the UV-complete QCD-like theory contains the left- and right-handed T-quark states $Q_{L/R} = (U, D, S)_{L/R}$ which are triplets under the flavour symmetry group $SU(3)_{\mathrm{L}} \otimes SU(3)_{\mathrm{R}}$ and where the Dirac U and D T-quarks are also charged under the EW symmetry. The corresponding scalar technihadron spectrum automatically contains two SM-like Higgs doublets $\mathcal{H}$ and $\mathcal{K}$ with a T-quark content $\begin{pmatrix} U\bar{S} & D\bar{S} \end{pmatrix}$. In order to describe the interactions and the mass spectrum of the scalar technihadrons, in full analogy with QCD, we implement the linear sigma model (LσM) approach, which, as shown in a previous work [17], leads to an overall consistency with the EW precision tests and with SM-like Higgs signal in the diphoton invariant mass spectrum. Chiral and EW symmetries are broken by T-quark condensates of different kind at $\Lambda_{\mathrm{TC}} \sim \mathcal{O}(1 - 10$ TeV) and $\Lambda_{EW} \sim \mathcal{O}(100\,\mathrm{GeV})$ scales, which non-perturbatively

and dynamically trigger the Higgs and sigma scalar vacuum expectation values (VEV). The dynamical aspect of the symmetry breaking occurs through the generation of flavour-diagonal, $\langle 0| : \bar{Q}Q : |0\rangle$, and off-diagonal condensates, $\langle 0| : \bar{D}S + \bar{S}D : |0\rangle$. In order to be consistent with the SM Higgs sector, it is imperative to impose certain conditions on the scalar VEVs and the T-quark condensates. The model is built in the near-conformal limit where, similarly to QCD, the bare masses of the T-quarks are assumed to be much smaller than the confinement scale Λ_{TC}.

The thesis is organized as follows. In Section 2, we lay the theoretical foundations and introduce the vocabulary necessary for the understanding of the rest of the thesis. In Section 3, we demonstrate vector-like confinement under $SU(N_{\text{TC}})_{\text{TC}}$, with $N_{\text{TC}} = 2$, and define the Dirac T-quarks. In Section 4, a new UV-complete strongly confined QCD-like composite Higgs model is built and chiral/EW symmetry breaking is demonstrated. The potential is then expanded to include Coleman-Weinberg (CW) radiative corrections as well as thermal corrections. In Section 5, the results from the computer models are presented and discussed. We end with Section 6 where a summary is given as well as prospects for further studies.

2 Building the framework

2.1 Technicolor

As Susskind wrote in 1984, there are two possible solutions to the gauge hierarchy problem — to either develop a novel gauge theory (a promising candidate being supersymmetry), or to study TC [18]. Evidently, we take the latter approach. The pioneering papers on the topic are those by Weinberg [19] and Susskind [5] who argued that a fundamental scalar in the theory poses a serious problem by disobeying the naturalness criterion. The idea behind TC is to avoid introducing such elementary scalars, as done in the SM, and break dynamically EW and chiral symmetries. If true, such models have the potential to give rise to exciting new physics.

Let us introduce this new gauge sector sitting at energies in the TeV range. The components of this sector are a set of T-quarks, carrying a new charge called TC. If there are a total of N_{TC} charges, then the gauge group of the theory is $G_{\text{TC}} = SU(N_{\text{TC}})_{\text{TC}}$, resulting in $N_{\text{TC}}^2 - 1$ gauge bosons that we, analogously to QCD, call technigluons. Let us also introduce an N_{Tf} number of flavours of chirally symmetric (Dirac) T-quarks whose left and right components belong to representations of the global chiral symmetry $SU(N_{\text{Tf}})_{\text{L}} \otimes SU(N_{\text{Tf}})_{\text{R}} \otimes U(1)_{\text{Y}}$. Its breaking then implies the existence of $N_{\text{Tf}}^2 - 1$ pseudo-Goldstone states. Similarly to QCD, the T-quarks behave as asymptotically free particles above the Λ_{TC} confinement scale. This new sector gives rise to additional gauge interactions as well as new technihadron bound

states — technimesons (T-mesons) and technibaryons [20].

Throughout the years, the plethora of TC models has only been growing [20]. Prior to the experimental discovery of the Higgs boson, many physicists have attempted to describe the dynamical breaking of the EW sector by excluding the Higgs field and instead invoking additional gauge interactions and extra dimensions [21]. The question now, however, is not whether the Higgs boson exists but whether it is indeed a fundamental scalar or rather a composite particle.

2.2 Electroweak phase transition

Phase transitions can be observed in many-particle systems as a result of the change of some physical quantity, to be introduced shortly, which we call the order parameter. In the context of EWPTs, the system transitions from obeying an $SU(2)_{\mathrm{W}} \otimes U(1)_{\mathrm{Y}}$ symmetry (Phase I) to being broken with respect to that symmetry group (Phase II). In our consideration, the order parameter concerns the change in VEV of the Higgs field from zero in Phase I, when temperatures are extreme but finite, to non-zero in Phase II when temperatures are considered to be zero. Such temperature changes result in the formation of bubbles of the broken-symmetry phase within the symmetric phase in a process known as nucleation, depicted in Figure 1 [22]. These bubbles grow until eventually all of space transitions to Phase II.

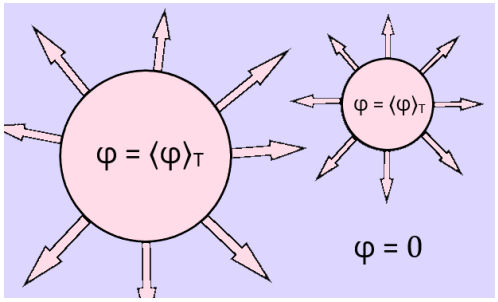

Figure 1: The process of nucleation where bubbles of the new phase start forming and eventually occupy all of space. These bubbles are associated with a radius and a wall speed.

A useful quantity for studying EWPTs turns out to be the free energy (upper-case letters) and the free energy density (lower-case letters) of a system given by

$$F = E - TS \qquad f = \rho - Ts,$$

where T is the temperature and E and S (ρ and s) are the internal energy and entropy (densities), respectively. The most favourable state for a system is described by the minimum of this function. Since the entropy density for relativistic particles is given by

$$s = \frac{p + \rho}{T},$$

the free energy density becomes simply equal to $(-p)$ and that quantity we shall calculate later in this section and use to compute the effective potential at a finite temperature.

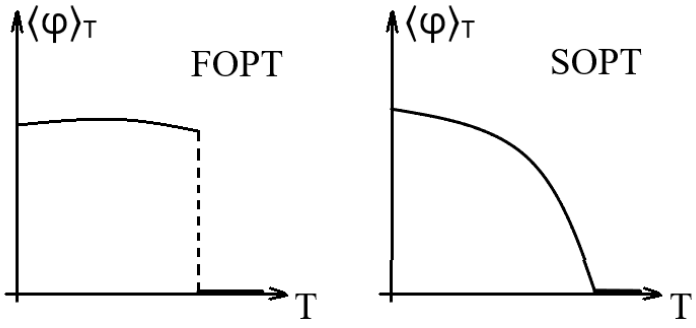

Figure 2: On the left figure, a FOPT is shown where the Higgs VEV drops rapidly with increasing temperature. Conversely, on the right figure, a SOPT is presented where the value of the Higgs VEV decreases smoothly as temperature increases.

Phase transitions are categorized into FOPTs and SOPTs. To give meaning to these categories, we first need to introduce the effective potential of the theory, $V_{\text{eff}}(\varphi)$. It is defined as the free energy density of a medium at a *finite* temperature and having a minimum expectation value at $\langle\varphi\rangle_T$. At zero temperature, the $SU(2)_{\text{W}} \otimes U(1)_{\text{Y}}$ symmetry of the potential is broken either abruptly or smoothly, corresponding to a FOPT and a SOPT, respectively. As shown in Figure 2, the difference between the two cases is described by the way $\langle\varphi\rangle_T$ changes with temperature. As the name suggests, EWPTs happen at temperature scales of $T \sim \{m_W, m_Z\} \approx 100\,\text{GeV}$ where m_W and m_Z are the masses of the $W^{\pm}$ and Z bosons, respectively. In what follows, we are going to consider the one-loop approximation calculation to the scalar potential and we are going to build the formalism used later in the thesis. We follow closely the calculations made in [23].

Up to leading order in perturbation theory, there are three contributions to the effective potential that ought to be considered, namely

$$V_{\text{eff}}(\varphi, T) = V_{\text{tree}} + V_{\text{CW}} + \Delta V. \tag{2.1}$$

Here, V_{tree} is the zero-temperature scalar potential at tree level

$$V_{\text{tree}}(\varphi) = \lambda \left(\varphi^2 - v_{\text{EW}}^2\right)^2,$$

where φ denotes the Higgs field, λ is the Higgs self-coupling constant and $v_{\text{EW}} = \langle\varphi\rangle_{T=0}$ is the Higgs VEV obtained by applying a minimization condition on the potential with respect to φ. The second term is the temperature-independent part of the one-loop radiative correction given by the CW potential [24]

$$V_{\text{CW}}(\varphi) = \sum_i (-1)^F g_i \frac{m_i^4}{64\pi^2} \left(\log\left[\frac{m_i^2(\varphi)}{\Lambda^2}\right] - c_i \right), \tag{2.2}$$

where $F = 0$ (1) for bosons (fermions), m_i is the mass of the i^{th} particle, g_i is the number of degrees of freedom of the i^{th} particle

$$g_W = 2 \cdot 3 = 6 \qquad g_Z = 3 \qquad g_{t,b} = 2 \cdot 2 \cdot 3 = 12 \qquad g_\tau = 2 \cdot 2 = 4, \tag{2.3}$$

$\Lambda = v_{\rm EW}^2$ is a renormalization scale and the constant c_i takes either of the two values $-\frac{3}{2}$ for scalars, fermions and longitudinally polarized gauge bosons or $\frac{1}{2}$ for transversely polarized gauge bosons [25]. Finally, the temperature contribution, $\Delta V(T)$, comes from the pressure, $(-p_i)$, exerted by an (anti-)particle i in the medium that couples to the SM Higgs. It bears the form

$$\sum_i (-p_i) = -\frac{1}{6\pi^2}\sum_i g_i \int_0^\infty \frac{k^4\, dk}{\sqrt{k^2+m_i^2}} \frac{1}{e^{\frac{\sqrt{k^2+m_i^2}}{T}} \mp 1},$$

where k is the four-momentum of the particle, m_i is the respective mass and the minus/plus sign corresponds to bosons/fermions. We then normalize m and k with respect to temperature, define the mass as proportional to the Higgs field

$$m_i = h_i \varphi$$

and evaluate the integral above (as done in Section A) to obtain the pressure term

$$-p_i = \frac{T^2}{24}\left[\sum_{\rm bosons} g_i h_i^2 \varphi^2 + \frac{1}{2}\sum_{\rm fermions} g_i h_i^2 \varphi^2\right],$$

where the sum over i is implied.

Another contribution to the thermal corrections comes from the masses of the (pseudo)-scalar sector that emerges from the theory. These are given by evaluating the Hessian matrix of the scalar potential

$$M^2 = \frac{\partial^2 V_{\rm tree}}{\partial \varphi^2}. \tag{2.4}$$

The final form of effective potential from eq. (2.1) is then

$$\begin{aligned} V_{\rm eff}(\varphi, T) = \lambda\left(\varphi^2 - v_{\rm EW}^2\right)^2 + \sum_i (-1)^F g_i \frac{(h_i\varphi)^4}{64\pi^2}\left(\log\left[\frac{(h_i\varphi)^2}{\Lambda^2}\right] - c_i\right) + \\ + \frac{T^2}{24}\left[{\rm Tr}(M^2) + \sum_{\rm bosons} g_i h_i^2 \varphi^2 + \frac{1}{2}\sum_{\rm fermions} g_i h_i^2 \varphi^2\right]. \end{aligned} \tag{2.5}$$

As shown in Figure 3, at non-zero temperatures, the effective potential acquires additional contributions that restore the symmetry of the potential and as a result the field's VEV becomes zero.

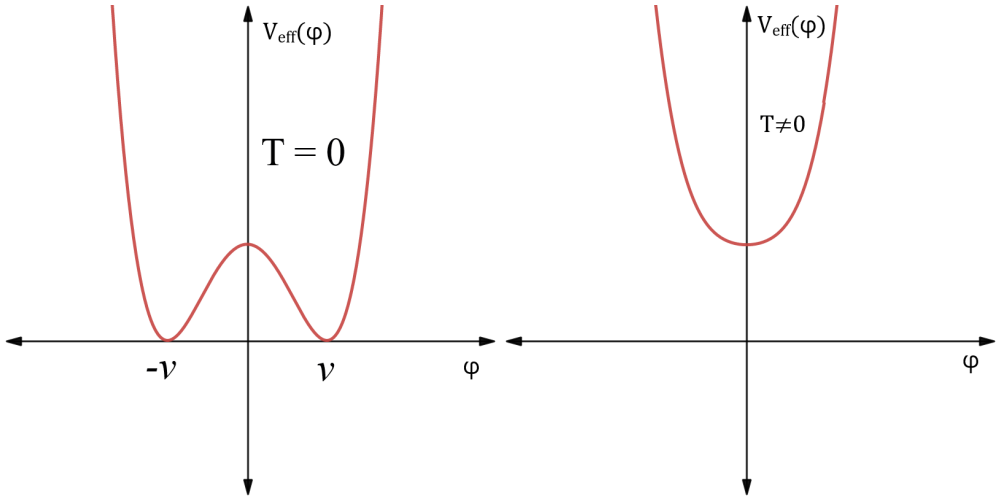

Figure 3: The φ potential at zero (left) and at non-zero (right) temperature.

2.3 Gravitational waves

Some 10^{-11} s after the inflationary and post-inflationary reheating phases[1] of the newly-born Universe, when temperatures had taken values of $\mathcal{O}(100\,\mathrm{GeV})$, a period of an EWPT followed. This is a time in the history of the Universe which we cannot observe directly from photon emissions. They could not escape the scattering off electrons and the absorption by hydrogen atoms — the rest of the Universe was opaque to light. It would take another 370 000 years for the electromagnetic waves to be able to escape and billions of years more to be detected as a cosmic microwave background radiation. Fortunately, there is another type of waves that is not affected by interactions of such nature — gravitational waves. In a recent paper [26], scientists discuss the very promising possibility of probing the theory by detecting stochastic signals from the nucleation of bubbles of the new phase that have been formed and expanded during the FOPTs process. This could be achieved using the state-of-the-art LISA interferometer [27] which is to be launched in the next decade.

The power spectrum of a stochastic gravitational wave background is statistically isotropic, stationary and Gaussian and is defined as a function of the gravitational wave frequency in the following way [25]

$$h^2\Omega_{\mathrm{GW}}(f) \equiv \frac{h^2}{\rho_c}\frac{\partial\rho_{\mathrm{GW}}}{\partial \log f},$$

where ρ_c is the critical energy density of the Universe at present times, ρ_{GW} is the energy density of the gravitational wave radiation and h is a dimensionless quantity parametrizing

[1]Inflation is a pre-Hot-Big-Bang period when the Universe experiences an exponential growth. Such a process could explain why the Universe we observe today is homogeneous, isotropic and flat. In the process that followed, post-inflationary reheating, the energy from the inflation is transferred to ordinary matter which as a result heats up and leads to a Hot Big Bang [23].

the value of the Hubble expansion rate such that

$$H_0 = h \cdot 100 \ \frac{\text{km}}{\text{s} \cdot \text{Mpc}}, \qquad h = 0.674(5) \ [28].$$

Gravitational waves from FOPTs could be produced as a result of three different events with their respective contributions to the gravitational wave background [29]

$$h^2\Omega_{\text{GW}} \simeq h^2\Omega_\phi + h^2\Omega_{\text{SW}} + h^2\Omega_{\text{MHD}}. \tag{2.6}$$

The first contribution in eq. (2.6) is due to collisions of bubbles and plasma shocks associated with Ω_ϕ. Such collisions could only give a significant contribution if the bubble walls are accelerated close to the speed of light (a phenomenon called "runaway bubbles"). However, the hot plasma in which the bubbles are expanding could create friction and prevent reaching such high velocities [30]. We therefore turn to the second contribution which comes from collisional sound waves, Ω_{SW}. This is where most of the energy would be dissipated and is the mechanism that is taken into account in this study. The third final and also very poorly understood[2] source of stochastic gravitational waves is plasma magnetohydrodynamic turbulence, Ω_{MHD}, that has formed after the collision of bubbles. We mention this contribution simply for completeness and it would not enter the equations stated below.

2.3.1 Equilibrium properties of the plasma

We now introduce the standard notation and procedure for analysing the gravitational wave spectrum. The bubble nucleation rate (per unit volume per unit time) is given by the Arrhenius formula [31] which reads

$$\Gamma(t) = A(t)e^{-\hat{S}_3(t)/T}, \tag{2.7}$$

where $A(t) \sim T^4$ is a pre-exponential factor. The parameter $\hat{S}_3$ is the Euclidean O(3)-symmetric action [32]

$$\hat{S}_3(\hat{\phi}, T) = 4\pi \int_0^\infty dr \ r^2 \left\{ \frac{1}{2} \left(\frac{d\hat{\phi}}{dr} \right)^2 + V_{\text{eff}}(\hat{\phi}, T) \right\}$$

which describes the expansion of the bubble in the limit $T \gg R_0$, where R_0^{-1} is the bubble radius. This coincides with an action of a particle moving in the external potential $U = -V_{\text{eff}}$, where r plays the role of time. The plus sign in front of the potential is due to the action being three-dimensional in the considering limit where the Euclidean time

[2]This contribution has large uncertainties but is also expected to be small compared to the sound-wave term, so we neglect it in this consideration following [25].

dependence $\tau = -it$ has been integrated out. The first important parameter in this analysis is the *nucleation rate parameter* (or also the *inverse time duration*) which is defined as

$$\beta(t) = \frac{d \ln \Gamma(t)}{dt} = \frac{d \ln \left[A(t) e^{-\hat{S}_3(t)/T} \right]}{dt} = \frac{\dot{A}}{A} - \frac{\dot{\hat{S}}_3}{T} = \frac{\dot{\Gamma}}{\Gamma}.$$

At the scales of EWPT, $\hat{S}_3(T_n)/T_n \simeq 140$, where T_n is the nucleation temperature [26]. Since most of the variation in eq. (2.7) with respect to time is in the $\hat{S}_3(t)$ term [33], the expression above can be very well approximated by

$$\beta(t) = \frac{\dot{\Gamma}}{\Gamma} \approx -\frac{d}{dt}\left(\frac{\hat{S}_3}{T}\right) \tag{2.8}$$

and in the expressions to follow we use equality instead of an approximation sign. We now perform a change of variables relating the Hubble time t to the temperature T at that time (Section B)

$$t = \frac{1}{2H} = \frac{1}{2CT^2},$$

where $H = CT^2$ is the Hubble parameter and

$$\frac{1}{C} = M_{\rm Pl}^* = \frac{M_{\rm Pl}}{1.66\sqrt{g_*}}, \qquad g_* \simeq 106.75$$

is the reduced Planck mass[3]. Then

$$dt = d\left(\frac{C^{-1}T^{-2}}{2}\right) = \frac{C^{-1}d\left(T^{-2}\right)}{2} = \frac{-\cancel{2}C^{-1}T^{-3}dT}{\cancel{2}} = -(CT^3)^{-1}dT.$$

Substituting the time differential with the temperature one, eq. (2.8) becomes

$$\frac{\beta}{CT^2} = T\,\frac{d}{dT}\left(\frac{\hat{S}_3}{T}\right).$$

Finally, remembering the definition of H introduced above, we arrive at the final form of the expression

$$\frac{\beta}{H} = T_n\,\frac{d}{dT}\left(\frac{\hat{S}_3}{T}\right)\Bigg|_{T=T_n}. \tag{2.9}$$

As pointed out in [33], one can arrive at the same result by using the adiabaticity of the Universe, namely perform the substitution $dT/dt = -TH$. In eq. (2.9), we have normalized the duration of the phase transition, β^{-1}, to the cosmological expansion time scale, H^{-1}. A smaller β/H, therefore, corresponds to a longer phase-transition on the time scale of the evolution of the Universe. As we point out later in Section 5, a trend is observed in which the value of eq. (2.9) decreases with increasing strength of the phase transition.

[3]At temperatures higher than 200 GeV, the contributions to the effective number of relativistic degrees of freedom comes from $g_* = 2_\gamma + 6_W + 3_Z + 1_h + 8^{(c)} \cdot 2_g + \frac{7}{8}(12_e + 6_\nu + 6 \cdot 3^{(c)} \cdot 4_q)$ [23].

2.3.2 Microscopic properties of the plasma

Another important parameter that enters the discussion is the *wall velocity*, v_w — the speed of the bubble wall in the rest frame of the plasma. Three different velocity profiles are possible depending on the value of v_w — deflagration, detonation and a hybrid (see [34] for a thorough review). The first one concerns wall velocities below the speed of sound, c_s, in the relativistic plasma. These play an important role in the process of EW baryogenesis. In this study, we concentrate on the second mechanism, detonation, for which v_w is larger than $c_s = \frac{1}{\sqrt{3}}$. There is a good reason for this choice. In order for the production of gravitational waves at the time of the phase transition to be significant, a large kinetic energy budget of EWPTs should be present at the boundaries and supersonic velocities are a necessary condition for that. Such gravitational waves will also be within LISA's detection range [35].

Obtaining an expression for v_w could become quite involved as it depends, amongst other things, on the friction generated by the plasma. What gives contribution to the friction are particles whose mass undergoes changes during the phase transition. This then makes the calculation very model-dependent [36]. Fortunately, in the supersonic regime we are interested in, we could safely impose the condition that v_w should be far from the Chapman-Jouguet speed [37, 38]

$$v_w > v_{\mathrm{CJ}} = \frac{1}{1+\alpha}\left(c_s + \sqrt{\alpha^2 + \frac{2}{3}\alpha}\right), \tag{2.10}$$

where α is the strength of the phase transition, to be defined in Section 2.3.3.

The expression for the nucleation rate parameter, eq. (2.9), gives an estimate of the typical size of a bubble, R. A reasonable starting point is to say that this parameter should be in some way proportional to the speed of the bubble wall and the duration of the phase transition. Moreover, since β serves as an inverse time duration, we can write that [39]

$$R \propto v_w \tau \approx \frac{v_w}{\beta}.$$

Upon maximizing the bubble volume distribution, one obtains

$$R = \frac{(8\pi)^{1/3}}{\beta}\max(v_w, c_s).$$

With these definitions, we can write down an expression describing the peak frequency of the gravitational wave [26, 25]

$$f_{\mathrm{peak}} = 26 \times 10^{-6}\left(\frac{1}{H_n R}\right)\left(\frac{T_n}{100}\right)\left(\frac{g_*}{100\,\mathrm{GeV}}\right)^{1/6}\ \mathrm{Hz}$$

while making the assumption that the percolation and nucleation temperatures are approximately equal, that the phase transition undergoes detonation and that the contributions from $h^2\Omega_\phi$ and $h^2\Omega_{\mathrm{MHD}}$ to the gravitational wave background are suppressed.

2.3.3 Hydrodynamical properties of the plasma

To avoid confusion, let us summarise the notation that we give to the energy densities that enter the discussion as done in [40]. Firstly, we make the assumption that the total energy in the Universe before nucleation comes from two contributions

$$\rho_{\rm tot} = \frac{3}{8\pi G} H_n^2 = \rho_\gamma + \rho_{\rm vac},$$

where the first equality comes from the Friedmann equation. The former and the latter terms in the second equality are the total radiation density in the symmetric phase and the false vacuum energy density from the scalar field potential (the *latent heat*), respectively. During the phase transition, the latter splits into three components: the gradient energy density of the scalar potential field ϕ, ρ_ϕ, the bulk kinetic energy density (the latent heat), ρ_v, and the thermal energy density, $\rho_{\rm th}$

$$\rho_{\rm tot} = \rho_\gamma + \rho_\phi + \rho_v + \rho_{\rm th}.$$

With this in mind, the ratios of different energy densities are formed. The first one is the *strength of the PT* given by

$$\alpha = \frac{\rho_{\rm vac}}{\rho_\gamma} = \frac{\Delta\theta(T)}{\rho_\gamma(T)} \tag{2.11}$$

with $\Delta\theta = \theta_s - \theta_b$ being the difference in the trace anomalies (traces of the energy-momentum tensor) between the symmetric (subscript s) and the broken phase (subscript b) [30]. The numerator is defined in terms of the potential energy difference

$$\Delta V = V_s - V_b = V(\phi = 0, T) - V(\phi = \phi_b, T)$$

in the following way

$$\Delta\theta(T) = \Delta V - \frac{T}{4}\frac{d\Delta V}{dT}.$$

The denominator is given by

$$\rho_\gamma = g_* \frac{\pi^2}{30} T_n^4$$

for a relativistic bosonic plasma[4]. The parameter can also be defined more intuitively as the ratio between the false vacuum energy density released during the transition and ρ_γ.

The other two ratios are the *efficiency parameters* given by the fraction of vacuum energy that gets converted into 1) gradient energy of ϕ and 2) fluid kinetic energy

$$\kappa_\phi = \frac{\rho_\phi}{\rho_{\rm vac}} \qquad \kappa_v = \frac{\rho_v}{\rho_{\rm vac}}.$$

[4]A derivation of this expression can be found, for example, in [23].

The from of κ_v is given in [25] and shall simply be stated here

$$\kappa = \frac{(v_{\rm CJ}-1)^3\ v_{\rm CJ}^{-5/2}\ v_w^{-5/2}\ \kappa_1\ \kappa_2}{L[(v_{\rm CJ}-1)^3-(v_w-1)^3R]\ v_{\rm CJ}^{5/2}\ \kappa_1+(v_w-1)^3\ \kappa_2},$$

where the efficiency factors are given by

$$\kappa_1 = \frac{\sqrt{\alpha}}{0.135+\sqrt{0.98+\alpha}}$$
$$\kappa_2 = \frac{\alpha}{0.73+0.083\sqrt{\alpha}+\alpha}$$

and the Chapman-Jouguet speed $v_{\rm CJ}$ is defined in eq. (2.10).

Lastly, using the results in [26], the kinetic energy fraction (the energy budget of the phase transition) is given by

$$K = \frac{\kappa\alpha}{1+\alpha}.$$

2.4 The Linear Sigma Model

In the following thesis, the model is based on a LσM. This approach has considerable advantages over the non-LσM when it comes to studying gravitational waves from FOPTs due to thermal loop corrections. We follow closely the lectures given in [41].

To explain the operation of the LσM, we introduce the following notation. Let ψ be a fermion field, σ be a scalar and $\vec{\pi} = \begin{pmatrix}\pi^1 & \pi^2 & \pi^3\end{pmatrix}$ be a triplet of pseudoscalar fields. The linear-σ Lagrangian density is then given by:

$$\mathcal{L}_\sigma = \frac{1}{2}(\partial_\mu\sigma)^2 + \frac{1}{2}(\partial_\mu\pi^2)^2 - \frac{\mu^2}{2}(\sigma^2+\vec{\pi}^2) - \frac{\lambda}{4}(\sigma^2+\vec{\pi}^2)^2 + \bar{\psi}i\partial\!\!\!/\psi + g\bar{\psi}(\sigma + i\vec{\sigma}\cdot\vec{\pi})\psi.$$

Let us rewrite this Lagrangian in terms of the chiral components of ψ. It bears the form

$$\begin{aligned}\mathcal{L}_\sigma = \frac{1}{4}\mathrm{Tr}(\partial_\mu\Sigma^\dagger\partial^\mu\Sigma) - \frac{\mu^2}{4}\mathrm{Tr}(\Sigma^\dagger\Sigma) - \frac{\lambda}{16}\left[\mathrm{Tr}(\Sigma^\dagger\Sigma)\right]^2 + \\ + \bar{\psi}_L i\partial\!\!\!/\psi_L + \bar{\psi}_R i\partial\!\!\!/\psi_R + g\bar{\psi}_L\Sigma\psi_R + g\psi_L\Sigma^\dagger\bar{\psi}_R,\end{aligned} \tag{2.12}$$

where we have defined the Σ field

$$\Sigma = \sigma\mathbb{1} + i\vec{\sigma}\cdot\vec{\pi},$$

with $\vec{\sigma}$ being the Pauli matrices and where the following identity has been applied

$$\sigma^2+\vec{\pi}^2 = \frac{1}{2}\mathrm{Tr}(\Sigma^\dagger\Sigma).$$

For chiral symmetry to be present, we require the following transformation properties

$$\psi_{L/R} \to U_{L/R}\ \psi_{L/R} \qquad \Sigma \to U_L\ \Sigma\ U_R^\dagger,$$

where $U_{L/R}$ are arbitrary $SU(2)$ matrices bearing the general form

$$U_{L/R} = \exp(-i\ \alpha^a_{L/R}\ \sigma^a/2).$$

The invariance of the Lagrangian in eq. (2.12) under chiral transformations is accompanied by the respective Noether vector and axial-vector currents

$$V^k_\mu = \bar{\psi}\gamma_\mu \frac{\sigma^k}{2}\psi + \varepsilon^{klm}\pi^l\partial_\mu\pi^m$$
$$A^k_\mu = \bar{\psi}\gamma_\mu\gamma_5 \frac{\sigma^k}{2}\psi + \pi^k\partial\sigma - \sigma\partial_\mu\pi^k.$$

3 Transformation properties of T-quark fields

Conventional TC models are built in a similar fashion to the quark sector in the SM. This means that 1) the left-handed T-quark fields $Q_L = \begin{pmatrix} U & D \end{pmatrix}_L$ in the fundamental representation of the $SU(N_{\rm TC})_{\rm TC} \otimes SU(2)_{\rm W} \otimes U(1)_{\rm Y}$ group and 2) the right-handed T-quark fields U_R and D_R in the fundamental representation of the $SU(N_{\rm TC})_{\rm TC} \otimes U(1)_{\rm Y}$ symmetry group obey different properties with respect to EW interactions. Following very closely the treatment in [42], we demonstrate how a chirally-symmetric TC model with $N_{\rm TC}$ can be constructed.

In this simplified description, we consider only the lightest T-quarks for the case of $N_{\rm TC} = 2$

$$Q_{L(A)} = \begin{pmatrix} U_{L(A)} & D_{L(A)} \end{pmatrix}, \qquad U_{R(1)}, D_{R(1)},$$

where $A = 1, 2$ denotes the number of generations, $Q_{L(A)}$ is a doublet under $SU(2)_{\rm W}$ and $U_{R(1)}, D_{R(1)}$ are singlets under the same group. The T-quarks are confined under the $SU(2)_{\rm W}$ symmetry group at a scale $\Lambda_{\rm TC} \gtrsim 1\,\text{TeV}$. With a hypercharge of zero and in complete analogy to SM hadron physics, the transformation property of the $SU(2)_{\rm W}$ doublets under $SU(2)_{\rm W} \otimes SU(2)_{\rm TC}$ is given by:

$$Q^{a\alpha'}_{L(A)} = Q^{a\alpha}_{L(A)} + \frac{i}{2}g_W\theta_k\tau^{ab}_k Q^{b\alpha}_{L(A)} + \frac{i}{2}g_{\rm TC}\varphi_k\tau^{\alpha\beta}_k Q^{a\beta}_{L(A)}, \tag{3.1}$$

where $a = 1, 2$ is the index of the fundamental representation of the weak isospin $SU(2)_{\rm W}$ group, $\alpha = 1, 2$ is the index of fundamental representation of the T-strong $SU(2)_{\rm TC}$ group. The transformation properties of the $SU(2)_{\rm W}$ singlets (denoted by a subscript "s") are instead given by:

$$U^{\alpha'}_{sR} = U^\alpha_{sR} - \frac{i}{2}g_1\theta U^\alpha_{sR} + \frac{i}{2}g_{\rm TC}\varphi_k\tau^{\alpha\beta}_k U^\beta_{sR}$$
$$D^{\alpha'}_{sR} = D^\alpha_{sR} + \frac{i}{2}g_1\theta D^\alpha_{sR} + \frac{i}{2}g_{\rm TC}\varphi_k\tau^{\alpha\beta}_k D^\beta_{sR}.$$

3.1 The $SU(2)_{\mathbf{W}} \otimes SU(2)_{\mathbf{TC}}$ group representation

In what follows, we keep the first generation of T-quarks unchanged. Let the doublet undergo charge conjugation and let us denote this transformation as $Q^{a\alpha}_{L(2)} \to Q^{Ca\alpha}_{L(2)}$. A right-handed second generation T-quark can then be obtained through

$$Q^{a\alpha}_{R(2)} = \varepsilon^{ab}\varepsilon^{\alpha\beta}Q^{Cb\beta}_{L(2)}, \tag{3.2}$$

where

$$\varepsilon^{ab} = \varepsilon^{\alpha\beta} = \begin{pmatrix} 0 & 1 \\ -1 & 0 \end{pmatrix}.$$

The two-dimensional Levi-Civita tensor defined above has the following properties

$$\varepsilon^{ij} = -\varepsilon^{ji} \qquad \varepsilon^{ii} = \varepsilon^{jj} = 0 \qquad i,j = 1,2. \tag{3.3}$$

The transformed conjugated left-handed field then reads

$$Q^{Ca\alpha'}_{L(2)} = Q^{Ca\alpha}_{L(2)} - \frac{i}{2}g_W\theta_k(\tau_k^{ab})^* Q^{Cb\alpha}_{L(2)} - \frac{i}{2}g_{\mathrm{TC}}\varphi_k(\tau_k^{\alpha\beta})^* Q^{Ca\beta}_{L(2)}.$$

The right-handed T-quark is analogously transformed as

$$\varepsilon^{ab}\varepsilon^{\alpha\beta}Q^{Cb\beta'}_{L(2)} = \varepsilon^{ab}\varepsilon^{\alpha\beta}Q^{Cb\beta}_{L(2)} - \frac{i}{2}g_W\theta_k\varepsilon^{ab}(\tau_k^{bc})^*\varepsilon^{\alpha\beta}Q^{Cc\beta}_{L(2)} - \frac{i}{2}g_{\mathrm{TC}}\varphi_k\varepsilon^{\alpha\beta}(\tau_k^{\beta\gamma})^*\varepsilon^{ab}Q^{Cb\gamma}_{L(2)}. \tag{3.4}$$

For the second and third terms on the RHS, we use the relations

$$\delta^{cd} = \varepsilon^{cf}\varepsilon^{df} \qquad\qquad \delta^{\gamma\lambda} = \varepsilon^{\gamma\mu}\varepsilon^{\lambda\mu}$$
$$\varepsilon^{ab}(\tau_k^{bc})^*\varepsilon^{cf} = \tau_k^{af} \qquad\qquad \varepsilon^{\alpha\beta}(\tau_k^{\beta\gamma})^*\varepsilon^{\gamma\mu} = \tau_k^{\alpha\mu}$$

as well as the identities in eq. (3.3) to obtain

$$\begin{aligned}\varepsilon^{ab}(\tau_k^{bc})^*\varepsilon^{\alpha\beta}Q^{Cc\beta}_{L(2)} &= \varepsilon^{ab}(\tau_k^{bc})^*\varepsilon^{cf}\varepsilon^{df}\varepsilon^{\alpha\beta}Q^{Cd\beta}_{L(2)} = -\tau_k^{af}\varepsilon^{fd}\varepsilon^{\alpha\beta}Q^{Cd\beta}_{L(2)} = \\ &= -\tau_k^{ab}\varepsilon^{bd}\varepsilon^{\alpha\beta}Q^{Cd\beta}_{L(2)} = -\tau_k^{ab}Q^{Cb\alpha}_{R(2)}\end{aligned} \tag{3.5}$$

$$\begin{aligned}\varepsilon^{\alpha\beta}(\tau_k^{\beta\gamma})^*\varepsilon^{ab}Q^{Cb\gamma}_{L(2)} &= \varepsilon^{\alpha\beta}(\tau_k^{\beta\gamma})^*\varepsilon^{\gamma\mu}\varepsilon^{\lambda\mu}\varepsilon^{ab}Q^{Cb\lambda}_{L(2)} = -\tau_k^{\alpha\mu}\varepsilon^{\mu\lambda}\varepsilon^{ab}Q^{Cb\lambda}_{L(2)} = \\ &= -\tau_k^{\alpha\beta}\varepsilon^{\beta\lambda}\varepsilon^{ab}Q^{Cb\lambda}_{L(2)} = -\tau_k^{\alpha\beta}Q^{Ca\beta}_{R(2)}.\end{aligned} \tag{3.6}$$

Now, applying eq. (3.2), eq. (3.5) and eq. (3.6), we rewrite the relation in eq. (3.4) as

$$Q^{Ca\alpha'}_{R(2)} = Q^{Ca\alpha}_{R(2)} + \frac{i}{2}g_W\theta_k\tau_k^{ab}Q^{Cb\alpha}_{R(2)} + \frac{i}{2}g_{\mathrm{TC}}\varphi_k\tau_k^{ab}Q^{Cb\alpha}_{R(2)}.$$

Comparing this result to eq. (3.1), we notice that the transformation properties of a *right-handed* T-quark of *second* generation (i.e., a complex conjugated left-handed T-quark) are

identical to the transformation properties of a *left-handed* T-quark of *first* generation. This rather nice property allows us to construct a *vector-like generation* of Dirac T-quarks:

$$Q^{a\alpha} = Q^{a\alpha}_{L(1)} + Q^{a\alpha}_{R(2)} = Q^{a\alpha}_{L(1)} + \varepsilon^{ab}\varepsilon^{\alpha\beta}Q^{Cb\beta}_{L(2)} \tag{3.7}$$

$$Q = \begin{pmatrix} U^1 & U^2 \\ D^1 & D^2 \end{pmatrix} = \begin{pmatrix} U^1_{L(1)} + U^1_{R(2)} & U^2_{L(1)} + U^2_{R(2)} \\ D^1_{L(1)} + D^1_{R(2)} & D^2_{L(1)} + D^2_{R(2)} \end{pmatrix} = \begin{pmatrix} Q^{11}_{L(1)} + Q^{11}_{R(2)} & Q^{12}_{L(1)} + Q^{12}_{R(2)} \\ Q^{21}_{L(1)} + Q^{21}_{R(2)} & Q^{22}_{L(1)} + Q^{22}_{R(2)} \end{pmatrix} =$$

$$= \begin{pmatrix} Q^{11}_{L(1)} + Q^{C22}_{L(2)} & Q^{12}_{L(1)} - Q^{C21}_{L(2)} \\ Q^{21}_{L(1)} - Q^{C12}_{L(2)} & Q^{22}_{L(1)} + Q^{C11}_{L(2)} \end{pmatrix}.$$

3.2 The $U(1)_{\mathbf{Y}} \otimes SU(2)_{\mathbf{TC}}$ group representation

Let now D^{α}_{sR} remain unchanged and define the charge conjugation on the second $SU(2)_{\mathrm{W}}$ singlet as $U^{\alpha}_{sR} \to U^{C\alpha}_{sR}$. Analogously to the previous section, we transform the field in the following way

$$U^{C\alpha'}_{sR} = U^{C\alpha}_{sR} + \frac{i}{2}g_1\theta U^{C\alpha}_{sR} - \frac{i}{2}g_{\mathrm{TC}}\varphi_k\tau^{\alpha\beta}_k U^{C\beta}_{sR}$$

after which we transpose the field so that it bears the form

$$-\varepsilon^{\alpha\beta}U^{C\beta'}_{sR} = -\varepsilon^{\alpha\beta}U^{C\beta}_{sR} + \frac{i}{2}g_1\theta\left(-\varepsilon^{\alpha\beta}U^{C\beta}_{sR}\right) + \frac{i}{2}g_{\mathrm{TC}}\varphi_k\varepsilon^{\alpha\beta}\tau^{\beta\gamma}_k\varepsilon^{\gamma\delta}(-\varepsilon^{\delta\lambda}U^{C\lambda}_{sR}). \tag{3.8}$$

Applying the following definition to eq. (3.8)

$$D^{\alpha}_{sL} = -\varepsilon^{\alpha\beta}U^{C\beta}_{sR},$$

we obtain

$$D^{\alpha'}_{sL} = D^{\alpha}_{sL} + \frac{i}{2}g_1\theta D^{\alpha}_{sL} + \frac{i}{2}g_{\mathrm{TC}}\varphi_k\tau^{\alpha\beta}_k D^{\beta}_{sL}.$$

Therefore, the transformation properties of a *left-handed* D^{a}_{sL} field (i.e., a complex conjugated right-handed U^{a}_{sR} field) are identical to the ones of a *right-handed* D^{a}_{sR} field. Analogously to the previous subsection, this means that we can construct a single vector-like Dirac T-quark field over the $SU(2)_{\mathrm{W}}$ group:

$$D^{\alpha}_{s} = D^{\alpha}_{sL} + D^{\alpha}_{sR} = -\varepsilon^{\alpha\beta}U^{C\beta}_{sR} + D^{\alpha}_{sR}. \tag{3.9}$$

Combining eq. (3.7) and eq. (3.9) and defining $D^{\alpha}_{s} \equiv S^{\alpha}$, where "S" stands for a singlet T-quark under $SU(2)_{\mathrm{W}}$, we can write down the following set of equations:

$$Q^{a\alpha} = Q^{a\alpha}_{L(1)} + Q^{a\alpha}_{R(2)} = Q^{a\alpha}_{L(1)} + \varepsilon^{ab}\varepsilon^{\alpha\beta}Q^{Cb\beta}_{L(2)}$$

$$S^{\alpha} = S^{\alpha}_{L} + S^{\alpha}_{R} = -\varepsilon^{\alpha\beta}U^{C\beta}_{R} + S^{\alpha}_{R}.$$

As described in [17], the vector-like weak interactions between Dirac T-quarks and vector-like bosons protect the model from large T-quark contributions to the S, T and U EW parameters. This is in contrast with non-vector-like TC models which have been ruled out by EW precision tests.

3.3 A Technicolor Lagrangian

Let us assume a composite nature of the Higgs boson such that EW symmetry is broken dynamically — a process called dynamical EWSB. The Lagrangian of the theory then fundamentally consists of two parts

$$\mathcal{L} = \mathcal{L}_{\text{SM}} + \mathcal{L}_{\text{TC}},$$

where the first term is the conventional SM Lagrangian without a scalar Higgs sector. The second term is the TC Lagrangian which bears a similar form to the Largangian of QCD

$$\begin{aligned}\mathcal{L}_{\text{TC}} = -\frac{1}{4}T^n_{\mu\nu}T^{\mu\nu}_n + i\bar{Q}\gamma^\mu\left(\partial_\mu - \frac{i}{2}g_W W^A_\mu \tau_A - \frac{i}{2}g_{\text{TC}}T^n_\mu\tau_n\right)Q - m_Q\bar{Q}Q + \\ + i\bar{S}\gamma^\mu\left(\partial_\mu - \frac{i}{2}g_1 B_\mu - \frac{i}{2}g_{\text{TC}}T^n_\mu\tau_n\right)S - m_S\bar{S}S,\end{aligned}$$

where $T^n_{\mu\nu}$ is the T-gluon field strength tensor. Note that in the discussion above we have mathematically shown that left- and right-handed $SU(2)_{\text{TC}}$ Dirac T-quarks obey the same transformation properties, thereby constructing a set of a chirally-symmetric bi-doublet and a singlet. This has interesting consequences on the TC Lagrangian — the only mass terms that are allowed by this symmetry are m_Q and m_S. These masses are phenomenological parameters of the vector-like TC model.

4 QCD-like composite Higgs Model

Conventional TC non-LσMs suffer from great complexity and non-perturbativity. In this project, we employ a different approach by constructing a UV-complete LσM based on chirally-symmetric (or vector-like) interactions between T-quarks and EW bosons. The model does not contain fundamental scalars, so the SM Higgs is assumed to be of composite nature. It is built in complete analogy to ordinary QCD, adopting the same $SU(N_{\text{TC}} = 3)_{\text{TC}}$ symmetry group and giving the new bound states analogous and intuitive names.

Let us construct the following T-quark/antiquark triplets

$$\mathcal{Q}_{L/R} = \begin{pmatrix} U & D & S \end{pmatrix}_{L/R} \qquad \bar{Q}_{L/R} = \begin{pmatrix} \bar{U} \\ \bar{D} \\ \bar{S} \end{pmatrix}_{L/R}$$

obeying the transformation properties

$$\mathcal{Q}'_L = \left(1 + \frac{i}{2}\zeta_a\lambda_a\right)\mathcal{Q}_L \qquad \mathcal{Q}'_R = \left(1 + \frac{i}{2}\xi_a\lambda_a\right)\mathcal{Q}_R,$$

where ζ_a/ξ_a are the generators of the $SU(3)_{\mathrm{L/R}}$ symmetry groups. Deviating slightly from conventional hadron physics, we make the assumption that

$$m_S \simeq m_Q \ll \Lambda_{\mathrm{TC}}.$$

This is a necessary condition for the existence of the non-diagonal condensate

$$\langle 0| : \bar{D}S + \bar{S}D : |0\rangle$$

which plays a crucial role in the breaking of EW symmetry as it effectively replaces the VEV of the SM Higgs boson.

4.1 Scalar and pseudoscalar T-mesons

In complete analogy to the QCD hadron notation, the T-meson sector of the σ-model includes the following combinations of T-quark–T-antiquark pairs

$$\pi^+, \pi^0, \pi^-; \qquad K^+, K^0, \bar{K}^0, K^-; \qquad \eta, \eta'$$

and their corresponding even-chirality partners

$$a^+, a^0, a^-; \qquad H^+, H^0, \bar{H}^0, H^-; \qquad f, \sigma,$$

where π, K and η are pseudoscalar pseudo-Goldstone bosons, a, H and f are scalar T-mesons and σ and η' are scalar and pseudoscalar T-glueballs, respectively. These 18 fields in total form the bi-fundamental representation of the $SU(3)_{\mathrm{L}} \otimes SU(3)_{\mathrm{R}}$ group with transformation properties

$$\Phi^{i'}_\alpha = \Phi^i_\alpha + \frac{i}{2}\zeta_a\lambda^i_{(a)k}\Phi^k_\alpha - \frac{i}{2}\xi_a\lambda^\beta_{(a)\alpha}\Phi^i_\beta,$$

where the multiplet Φ^i_α bears the form

$$\hat{\Phi} = \frac{1}{\sqrt{2}}\begin{pmatrix} \frac{1}{\sqrt{2}}a^0 + \frac{1}{\sqrt{6}}f + \frac{1}{\sqrt{3}}\sigma & a^+ & H^+ \\ a^- & -\frac{1}{\sqrt{2}}a^0 + \frac{1}{\sqrt{6}}f + \frac{1}{\sqrt{3}}\sigma & H^0 \\ H^- & \bar{H}^0 & -\sqrt{\frac{2}{3}}f + \frac{1}{\sqrt{3}}\sigma \end{pmatrix} -$$
$$- \frac{i}{\sqrt{2}}\begin{pmatrix} \frac{1}{\sqrt{2}}\pi^0 + \frac{1}{\sqrt{6}}\eta + \frac{1}{\sqrt{3}}\eta' & \pi^+ & K^+ \\ \pi^- & -\frac{1}{\sqrt{2}}\pi^0 + \frac{1}{\sqrt{6}}\eta + \frac{1}{\sqrt{3}}\eta' & K^0 \\ K^- & \bar{K}^0 & -\sqrt{\frac{2}{3}}\eta + \frac{1}{\sqrt{3}}\eta' \end{pmatrix}. \qquad (4.1)$$

In the definition above, the Higgs sector is constructed from the following strongly coupled bound states:

$$\mathcal{H} = \begin{pmatrix} H^+ \\ H^0 \end{pmatrix} \qquad \mathcal{K} = \begin{pmatrix} K^+ \\ K^0 \end{pmatrix}.$$

We are now ready to construct the TCLσM Lagrangian:

$$\begin{aligned} \mathcal{L}_\sigma =& i\bar{\mathcal{Q}}\gamma^\mu\partial_\mu\mathcal{Q} + \partial_\mu\hat{\Phi}^\dagger\partial^\mu\hat{\Phi} + \\ &+ \mu^2\hat{\Phi}^\dagger\hat{\Phi} - \lambda_1\left(\hat{\Phi}^\dagger\hat{\Phi}\right)^2 - 3\lambda_2\hat{\Phi}^\dagger\hat{\Phi}\hat{\Phi}^\dagger\hat{\Phi} + 2\sqrt{6}\Lambda_3\mathrm{Re}\left(\det\,\hat{\Phi}\right) - \\ &- \sqrt{6}\varkappa\left(\bar{\mathcal{Q}}_L\hat{\Phi}\mathcal{Q}_R + \bar{\mathcal{Q}}_R\hat{\Phi}^\dagger\mathcal{Q}_L\right). \end{aligned} \tag{4.2}$$

The first line consists of kinetic terms involving only the derivatives of the fields. The second and third lines make up the potential energy density where the last term is the one responsible for the dynamical breaking of chiral and EW symmetries. In principle, plugging in the matrix from eq. (4.1) into eq. (4.2) without making any simplifications would result in an extremely complicated form of the Lagrangian. Minimizing the potential and calculating the extremum points would become a very ambitious task as it would require solving 18 coupled equations. Therefore, in what follows, we firstly give the σ field a VEV — an action that would break the chiral symmetry of the Lagrangian at Λ_{TC}. Later on, the $\mathcal{H}$ field would acquire a VEV, breaking dynamically the EW symmetry of the theory at a lower energy scale, Λ_{EW}.

4.2 Breaking chiral symmetry

Let us explore the consequences of giving the σ field a non-zero VEV

$$u = \langle 0|\sigma|0\rangle \neq 0$$

while keeping the VEVs of the rest of the fields zero. Plugging in eq. (4.1) into eq. (4.2) and expanding the potential terms, we obtain

$$U_{\mathrm{vac}} = -\frac{1}{2}\mu^2u^2 + \frac{1}{4}(\lambda_1+\lambda_2)u^4 - \frac{1}{3}\Lambda_3u^3 + \varkappa u\langle 0|:\bar{\mathcal{Q}}\mathcal{Q}:|0\rangle,$$

where μ^2, λ_1, λ_2, Λ_3 and $\varkappa\langle 0|:\bar{Q}Q:|0\rangle$ are independent parameters and

$$\langle 0|:\bar{Q}Q:|0\rangle = \langle 0|:\bar{U}_LU_R + \bar{U}_RU_L + \bar{D}_LD_R + \bar{D}_RD_L + \bar{S}_LS_R + \bar{S}_RS_L:|0\rangle$$

is the diagonal T-quark condensate.

We need to write down a set of equations which ensure that the potential has an extremum at $\langle\sigma\rangle = u$ and that this extremum is a minimum of the function. Such stability conditions

are straightforwardly obtained through differentiation

$$\frac{dU_{\rm vac}}{du} = u\left[-\mu^2 + (\lambda_1+\lambda_2)u^2 - \Lambda_3 u + \frac{\varkappa}{u}\langle 0|:\bar{\mathcal{Q}}\mathcal{Q}:|0\rangle\right] = 0 \tag{4.3}$$
$$\frac{d^2U_{\rm vac}}{d^2u} = 2(\lambda_1+\lambda_2)u^2 - \Lambda_3 u - \frac{\varkappa}{u}\langle 0|:\bar{\mathcal{Q}}\mathcal{Q}:|0\rangle > 0,$$

where we make use of the first equation to obtain the second one. Let us define the chiral-symmetry-breaking term as:

$$\theta = \varkappa\langle 0|:\bar{\mathcal{Q}}\mathcal{Q}:|0\rangle. \tag{4.4}$$

To obtain the mass spectrum, an 18×18 Hessian matrix is constructed using eq. (2.4). The matrix is evaluated at $\langle\sigma\rangle = u$ and at the value of μ^2 obtained from eq. (4.3). Diagonalizing the Hessian mass-squared matrix, all physical states are obtained and their mass spectrum is summarized below. The subscript (0) is a reminder that these are the masses-squared in the EW *unbroken* phase.

1. Pseudoscalar T-mesons:

$$M^2_{\pi(0)} = M^2_{K(0)} = M^2_{\eta(0)} = -\frac{\theta}{u}$$

2. Scalar T-mesons:

$$M^2_{a(0)} = M^2_{H(0)} = M^2_{f(0)} = 2\lambda_2 u^2 + 2\Lambda_3 u + M^2_{\pi(0)}$$

3. Scalar and pseudoscalar T-glueballs:

$$M^2_{\sigma(0)} = 2(\lambda_1+\lambda_2)u^2 - \Lambda_3 u + M^2_{\pi(0)}$$
$$M^2_{\eta'(0)} = 3\Lambda_3 u + M^2_{\pi(0)}$$

All free parameters can be expressed in terms of the squared masses as follows:

$$-\frac{\theta}{u} = M^2_{\pi(0)} \tag{4.5}$$
$$2\lambda_1 u^2 = M^2_{\sigma(0)} + M^2_{\eta'(0)} - (M^2_{H(0)} + M^2_{\pi(0)}) \tag{4.6}$$
$$2\lambda_2 u^2 = M^2_{H(0)} - \frac{1}{3}M^2_{\eta'(0)} + \frac{7}{3}M^2_{\pi(0)} - M^2_{\sigma(0)} \tag{4.7}$$
$$\Lambda_3 u = \frac{1}{3}(M^2_{\eta'(0)} - M^2_{\pi(0)}). \tag{4.8}$$

4.3 Breaking electroweak symmetry

While chiral symmetry is broken at energies of $\mathcal{O}(\Lambda_{\text{TC}})$, which is in the TeV range, dynamical EWSB happens at EW energy scales i.e., in the GeV regime where the mesons constituting the multiplet from eq. (4.1) are considered to be point-like particles as their intrinsic structure is no longer prominent. The T-hadrons have different hypercharge values as follows:

- the π and a T-meson triplets carry $Y_\pi = Y_a = 0$ and form adjoint representations of the $SU(2)_{\text{W}}$ group;
- the $\mathcal{H}$ and $\mathcal{K}$ T-meson doublets carry $Y_H = Y_K = \frac{1}{2}$ and form fundamental representations of the $SU(2)_{\text{W}}$ group;
- the rest of the T-mesons (η, η', f and σ) carry $Y_\eta = Y_{\eta'} = Y_f = Y_\sigma = 0$ and are singlets under the $SU(2)_{\text{W}}$ group.

This requires a slight modification to the kinetic terms of the Lagrangian from eq. (4.2)

$$\begin{aligned}\mathcal{L}_\sigma =& i\bar{\mathcal{Q}}\gamma^\mu\partial_\mu\mathcal{Q} + \partial_\mu\hat{\Phi}^\dagger\partial^\mu\hat{\Phi} + \\ &+ \frac{1}{2}\left(\mathcal{D}^\mu\pi_a\cdot\mathcal{D}_\mu\pi_a + \mathcal{D}^\mu a_a\cdot\mathcal{D}_\mu a_a\right) + \left(\mathcal{D}^\mu\mathcal{H}\right)^\dagger\cdot\mathcal{D}_\mu\mathcal{H} + \left(\mathcal{D}^\mu\mathcal{K}\right)^\dagger\cdot\mathcal{D}_\mu\mathcal{K} + \\ &+ \frac{1}{2}\left(\partial^\mu\eta\cdot\partial_\mu\eta + \partial^\mu\eta'\cdot\partial_\mu\eta' + \partial^\mu f\cdot\partial_\mu f + \partial^\mu\sigma\cdot\partial_\mu\sigma\right) + \\ &+ \mu^2\hat{\Phi}^\dagger\hat{\Phi} - \lambda_1\left(\hat{\Phi}^\dagger\hat{\Phi}\right)^2 - 3\lambda_2\hat{\Phi}^\dagger\hat{\Phi}\hat{\Phi}^\dagger\hat{\Phi} + 2\sqrt{6}\Lambda_3\text{Re}\left(\det\,\hat{\Phi}\right) - \\ &- \sqrt{6}\varkappa\left(\bar{\mathcal{Q}}_{_L}\hat{\Phi}\mathcal{Q}_{_R} + \bar{\mathcal{Q}}_{_R}\hat{\Phi}^\dagger\mathcal{Q}_{_L}\right),\end{aligned}$$

where the covariant derivatives are given by

$$\begin{aligned}\mathcal{D}_\mu\pi_a &= \partial_\mu\pi_a + g_{_W}\varepsilon_{abc}W^b_\mu\pi^c & \mathcal{D}_\mu a_a &= \partial_\mu a_a + g_{_W}\varepsilon_{abc}W^b_\mu a^c \\ \mathcal{D}_\mu\mathcal{K} &= \partial_\mu\mathcal{K} - \frac{i}{2}g_{_W}W^a_\mu\tau_a\mathcal{K} - \frac{i}{2}g_1B_\mu & \mathcal{D}_\mu\mathcal{H} &= \partial_\mu\mathcal{H} - \frac{i}{2}g_{_W}W^a_\mu\tau_a\mathcal{H} - \frac{i}{2}g_1B_\mu.\end{aligned}$$

For simplicity, in what follows, we are going to suppress the parameter μ^2.

Here and in the following Section 4.4, the σ as well as one of the Higgs doublets acquires a VEV such that

$$u = \langle 0|\sigma|0\rangle \quad \text{and} \quad \frac{v}{\sqrt{2}} \equiv \langle 0|H^0|0\rangle \quad \Rightarrow \quad \mathcal{H} = \frac{1}{\sqrt{2}}\begin{pmatrix}0\\ v\end{pmatrix}.$$

Applying the very same technique as in Section 4.2, the potential energy density term in eq. (4.2) is expanded and an additional symmetry breaking term appears

$$\omega \equiv \sqrt{\frac{3}{2}}\varkappa\langle 0| : \bar{D}S + \bar{S}D : |0\rangle, \tag{4.9}$$

where

$$\langle 0| : \bar{D}S + \bar{S}D : |0\rangle = \langle 0| : \bar{D}_L S_R + \bar{D}_R S_L + D_L \bar{S}_R + D_R \bar{S}_L : |0\rangle$$

is the off-diagonal T-quark condensate. We therefore obtain an expression of the form

$$U_{\text{vac}} = \frac{1}{4}(\lambda_1 + \lambda_2)(u^2 + v^2)^2 + \lambda_2 v^2 \left(u^2 + \frac{1}{8}v^2\right) + \Lambda_3 u \left(\frac{1}{2}v^2 - \frac{1}{3}u^2\right) + u\theta + v\omega.$$

Similarly to the previous discussion, the extremum points are given by

$$\frac{\partial U_{\text{vac}}}{\partial u} = u\left[(\lambda_1 + \lambda_2)(u^2 + v^2) + 2\lambda_2 v^2 + \Lambda_3\left(\frac{v^2}{2u} - u\right) + \frac{\theta}{u}\right] = 0 \tag{4.10}$$

$$\frac{\partial U_{\text{vac}}}{\partial v} = v\left[(\lambda_1 + \lambda_2)(u^2 + v^2) + \lambda_2\left(2u^2 + \frac{1}{2}v^2\right) + \Lambda_3 u + \frac{\omega}{v}\right] = 0. \tag{4.11}$$

Solving eq. (4.10) and eq. (4.11) for θ and ω, respectively, the condensates can be expressed in terms of the parameters λ_1, λ_2, Λ_3, u and v

$$\theta = -u(u^2 + v^2)\lambda_1 - u(u^2 + 3v^2)\lambda_2 + \left(u^2 - \frac{v^2}{2}\right)\Lambda_3 \tag{4.12}$$

$$\omega = -v(u^2 + v^2)\lambda_1 - 3v\left(u^2 + \frac{v^2}{2}\right)\lambda_2 - uv\Lambda_3. \tag{4.13}$$

The stability condition equation then takes the form

$$\Delta \equiv \frac{\partial^2 U_{\text{vac}}}{\partial u^2} \cdot \frac{\partial^2 U_{\text{vac}}}{\partial v^2} - \left(\frac{\partial^2 U_{\text{vac}}}{\partial u\, \partial v}\right)^2 > 0.$$

Let us define the ratio between the two VEVs to be

$$\delta = \frac{v}{u}.$$

The condition $\Delta > 0$ implies that $\delta \ll 1$ (neglecting orders of v higher than one). It is therefore required that the Higgs VEV takes values much smaller than the σ VEV. In this case, the model is described by the following mass scales

1. Pseudoscalar T-mesons:

$$M^2_{\pi(0)} = -u\Lambda_3 + u^2(\lambda_1 + \lambda_2)$$

2. Scalar T-mesons:

$$M^2_{H(0)} = u\Lambda_3 + u^2(\lambda_1 + 3\lambda_2)$$

3. Scalar and pseudoscalar T-glueballs:

$$M^2_{\sigma(0)} = -2u\Lambda_3 + 3u^2(\lambda_1 + \lambda_2)$$
$$M^2_{\eta'(0)} = 2u\Lambda_3 + u^2(\lambda_1 + \lambda_2).$$

In the limit of small δ, the masses calculated above are completely consistent with the ones obtained in eq. (4.6), eq. (4.7), eq. (4.8), where the parameters λ_1, λ_2 and Λ_3 are expressed as functions of the masses instead. In this limit, we can also write, using eq. (4.11), that

$$\frac{\omega}{v} = -\left[u^2(\lambda_1 + 3\lambda_2) + u\Lambda_3\right] - v^2\lambda_1 - \frac{3}{2}v^2\lambda_2.$$

We therefore obtain this interesting and rather trivial relation between the T-quark condensate in the TC theory and the SM values for the Higgs VEV and the Higgs boson mass:

$$\omega \simeq -vM^2_{H(0)} \simeq -(158\,\mathrm{GeV})^3.$$

4.4 Mass spectrum

In the following section, we construct the mass spectrum of the theory in terms of the mass scales $M^2_{\pi(0)}$, $M^2_{H(0)}$, $M^2_{\sigma(0)}$ and $M^2_{\eta'(0)}$. The calculations have been performed using the `Mathematica` software [43]. Each of the four cases of neutral and charged pseudoscalar and scalar T-mesons is considered. A similar discussion has been made in [17]. In the following, we add an additional order of magnitude to the precision compared to the previous calculation by including terms proportional to δ^2.

1. Neutral pseudoscalar T-mesons

   Let us define the following pseudoscalar field combinations

   $$\zeta = \frac{1}{\sqrt{2}}(K^0 + \bar{K}^0) \qquad \xi = \frac{i}{\sqrt{2}}(K^0 - \bar{K}^0).$$

   This definition turns out to be rather useful, as the ξ field is purely self-interacting and does not mix with any other fields. This would not contribute to the matrix M^2_{NPS} written down below — the only non-zero entry would be $M^2_{\mathrm{NPS},55}$. For the set of new neutral pseudoscalar fields

   $$\{\eta', \zeta, \eta, \pi^0\}$$

   the Hessian mass-squared matrix is given by

$$M^2_{\rm NPS} = \begin{pmatrix} 2M^2_{\eta'(0)} + \frac{2\chi_3}{3}\delta^2 & 2\chi_1\delta & \frac{\chi_6}{6\sqrt{2}}\delta^2 & \frac{\chi_6}{2\sqrt{6}}\delta^2 \\ 2\chi_1\delta & 2M^2_{\pi(0)} + \frac{\chi_4}{6}\delta^2 & \frac{\chi_2}{\sqrt{2}}\delta & \sqrt{\frac{3}{2}}\chi_2\delta \\ \frac{\chi_6}{6\sqrt{2}}\delta^2 & \frac{\chi_2}{\sqrt{2}}\delta & 2M^2_{\pi(0)} + \frac{\chi_5}{6}\delta^2 & \frac{\chi_6}{\sqrt{3}}\delta^2 \\ \frac{\chi_6}{2\sqrt{6}}\delta^2 & \sqrt{\frac{3}{2}}\chi_2\delta & \frac{\chi_6}{\sqrt{3}}\delta^2 & 2M^2_{\pi(0)} + \frac{\chi_4}{6}\delta^2 \end{pmatrix},$$

where

$$\chi_1 = M^2_{H(0)} - M^2_{\eta'(0)} \qquad \chi_2 = M^2_{\pi(0)} - M^2_{H(0)} \qquad \chi_3 = M^2_{\eta'(0)} + 2M^2_{\pi(0)}$$
$$\chi_4 = 2\chi_1 - \chi_2 + 4\chi_3 \qquad \chi_5 = 10\chi_1 - 5\chi_2 + 4\chi_3 \qquad \chi_6 = -2\chi_1 + \chi_2.$$

Upon calculating the eigenvalues of the matrix above, we obtain the following physical masses

$$M^2_{\eta'} = 2M^2_{\eta'(0)} + \frac{(3\chi_1^2 + M^2_{\eta'(0)}\chi_3 - M^2_{\pi(0)}\chi_3)}{3(M^2_{\eta'(0)} - M^2_{\pi(0)})}\delta^2 + \mathcal{O}(\delta^3)$$

$$M^2_{\zeta} = 2M^2_{\pi(0)} + \frac{\chi_4 + 3(\chi_5 - 4\chi_6)}{48}\delta^2 + \mathcal{O}(\delta^3)$$

$$M^2_{\eta} = 2M^2_{\pi(0)} - \frac{\chi_2}{\sqrt{2}}\delta + \frac{1}{96}\left(-\frac{48\chi_1^2}{M^2_{\eta'(0)} - M^2_{\pi(0)}} + 7\chi_4 + \chi_5 + 12\chi_6\right)\delta^2 + \mathcal{O}(\delta^3)$$

$$M^2_{\pi} = 2M^2_{\pi(0)} + \frac{\chi_2}{\sqrt{2}}\delta + \frac{1}{96}\left(-\frac{48\chi_1^2}{M^2_{\eta'(0)} - M^2_{\pi(0)}} + 7\chi_4 + \chi_5 + 12\chi_6\right)\delta^2 + \mathcal{O}(\delta^3)$$

$$M^2_{\xi} = 2M^2_{H(0)} + \frac{-2\chi_1 + \chi_2 - 4\chi_3}{6}\ \delta^2 + \mathcal{O}(\delta^3).$$

2. Neutral scalar T-mesons

   Very similarly to the treatment we applied for the neutral pseudoscalars, let us redefine the neutral scalar fields in the following way

$$h = \frac{1}{\sqrt{2}}(H^0 + \bar{H}^0) \qquad g = \frac{i}{\sqrt{2}}(H^0 - \bar{H}^0).$$

As expected, the g field is not mixing with any of the other neutral scalar fields. Therefore, its mass is obtained trivially by differentiating the potential twice with respect to that field. For the new set of fields

$$\{\sigma, h, a_0, f\}$$

the Hessian mass-squared matrix is given by

$$M^2_{\rm NS} = \begin{pmatrix} 2M^2_{\sigma(0)} - \frac{2\kappa_3}{3}\delta^2 & -\frac{2\kappa_1}{3}\delta & \frac{\kappa_5}{2\sqrt{6}}\delta^2 & \frac{\kappa_5}{6\sqrt{2}}\delta^2 \\ -\frac{2\kappa_1}{3}\delta & 2M^2_{H(0)} + \frac{\kappa_4}{2}\delta^2 & \frac{\kappa_2}{\sqrt{6}}\delta & \frac{\kappa_2}{3\sqrt{2}}\delta \\ \frac{\kappa_5}{2\sqrt{6}}\delta^2 & \frac{\kappa_2}{\sqrt{6}}\delta & M^2_{H(0)} + \frac{\kappa_4}{6}\delta^2 & 0 \\ \frac{\kappa_5}{6\sqrt{2}}\delta^2 & \frac{\kappa_2}{3\sqrt{2}}\delta & 0 & M^2_{H(0)} + \frac{\kappa_4}{6}\delta^2 \end{pmatrix},$$

where

$$\begin{aligned} \Delta^2_{\rm PS} &= M^2_{\eta'(0)} - M^2_{\pi(0)} \quad & \kappa_1 &= \Delta^2_{\rm PS} - 6M^2_{H(0)} \quad & \kappa_2 &= 7\Delta^2_{\rm PS} - 9M^2_{H(0)} + 3M^2_{\sigma(0)} \\ \kappa_3 &= \Delta^2_{\rm PS} - 3M^2_{H(0)} \quad & \kappa_4 &= 2\kappa_1 + \kappa_2 - 8\kappa_3 \quad & \kappa_5 &= 2\kappa_1 + \kappa_2 - 4\kappa_3. \end{aligned}$$

Upon diagonalizing the matrix and calculating the eigenvalues, the masses-squared of the fields are

$$M^2_\sigma = 2M^2_{\sigma(0)} - \frac{\kappa_1^2 + 6(M^2_{H(0)} - M^2_{\sigma(0)})\kappa_3}{9(M^2_{H(0)} - M^2_{\sigma(0)})}\ \delta^2 + \mathcal{O}(\delta^3)$$

$$M^2_h = 2M^2_{H(0)} + \frac{\kappa_4}{6}\ \delta^2 + \mathcal{O}(\delta^3)$$

$$M^2_{a_0} = 2M^2_{H(0)} - \frac{2\kappa_2}{3\sqrt{2}}\delta + \frac{\kappa_1^2 + 3(M^2_{H(0)} - M^2_{\sigma(0)})\kappa_4}{9(M^2_{H(0)} - M^2_{\sigma(0)})}\ \delta^2 + \mathcal{O}(\delta^3)$$

$$M^2_f = 2M^2_{H(0)} + \frac{2\kappa_2}{3\sqrt{2}}\delta + \frac{\kappa_1^2 + 3(M^2_{H(0)} - M^2_{\sigma(0)})\kappa_4}{9(M^2_{H(0)} - M^2_{\sigma(0)})}\ \delta^2 + \mathcal{O}(\delta^3)$$

$$M^2_g = 2M^2_{\pi(0)} - \frac{2\kappa_1 + \kappa_2}{6}\ \delta^2 + \mathcal{O}(\delta^3).$$

3. Charged (pseudo)scalar T-mesons

   The Hessian mass-squared matrices for the charged pseudoscalars $\{\pi^+, \pi^-, K^+, K^-\}$ and charged scalars $\{a^+, a^-, H^+, H^-\}$ is given as follows

$$M^2_{\mathrm{C(P)S}} = \begin{pmatrix} \Delta^2_{\mathrm{C(P)S}} + \psi_3\delta^2 & \psi_4 & \psi_1\delta & \psi_2\delta \\ \psi_4 & \Delta^2_{\mathrm{C(P)S}} + \psi_3\delta^2 & \psi_2\delta & \psi_1\delta \\ \psi_1\delta & \psi_2\delta & \Delta^2_{\mathrm{C(P)S}} + \psi_3\delta^2 & \psi_4 \\ \psi_2\delta & \psi_1\delta & \psi_4 & \Delta^2_{\mathrm{C(P)S}} + \psi_3\delta^2 \end{pmatrix},$$

   where

$$\psi_1 = 2\sqrt{6}u^2\lambda_2 \qquad \psi_2 = \pm\sqrt{6}u(-u\lambda_2 + \Lambda_3) \qquad \psi_3 = u^2(2\lambda_1 + 3\lambda_2)$$
$$\psi_4 = \mp 2u(u\lambda_2 + \Lambda_3) \qquad \Delta^2_{\mathrm{C(P)S}} = M^2_{\pi(0)} + M^2_{H(0)}$$

   and the upper and lower signs in ψ_2 and ψ_4 refer to pseudoscalars and scalars, respectively. The eigenvalues turn out to be

$$M^2_{\pi^\pm} = 2M^2_\pi - (\psi_1 + \psi_2)\delta + \psi_3\delta^2 + \mathcal{O}(\delta^3)$$
$$M^2_{K^\pm} = 2M^2_\pi + (\psi_1 + \psi_2)\delta + \psi_3\delta^2 + \mathcal{O}(\delta^3)$$
$$M^2_{a^\pm} = 2M^2_\pi - (\psi_1 + \psi_2)\delta + \psi_3\delta^2 + \mathcal{O}(\delta^3)$$
$$M^2_{H^\pm} = 2M^2_\pi + (\psi_1 + \psi_2)\delta + \psi_3\delta^2 + \mathcal{O}(\delta^3),$$

   where the respective signs in ψ_2 are respected for pseudoscalars $\{\pi^\pm, K^\pm\}$ and scalars $\{a^\pm, H^\pm\}$.

In the previous study [17], the phenomenology of the model has been thoroughly examined. It has been shown that the Higgs boson decay via the $\gamma\gamma$ channel very interestingly produces not one but two peaks which in the data of present-day colliders appear smeared out and seen as a single peak. These two peaks correspond to two states — the a_0 and the f T-mesons. Six pseudo-Goldstones show up as three distinct peaks at an energy level lower than 125 GeV which indicates that some states are overlapping. The η' and the σ appear as single peaks sitting at higher energy scales compared to the Higgs boson.

4.5 Tree-level potential and field-dependent masses

Let us define the singlet and the two Higgs doublets in terms of three classical background fields ϕ_σ, ϕ_h and ϕ_k

$$\sigma = \phi_\sigma \qquad \mathcal{H} = \frac{1}{\sqrt{2}}\begin{pmatrix}0\\ \phi_h\end{pmatrix} \qquad \mathcal{K} = \frac{1}{\sqrt{2}}\begin{pmatrix}0\\ \phi_k\end{pmatrix}.$$

We substitute the relations above into eq. (4.1) so that the multiplet is expressed in terms of the newly-defined fields. The term that gives rise to T-quark condensates now bears the form

$$\begin{aligned}\sqrt{6}\varkappa\left(\bar{\mathcal{Q}}_L\hat{\Phi}\mathcal{Q}_R + \bar{\mathcal{Q}}_R\hat{\Phi}^\dagger\mathcal{Q}_L\right) &= \kappa\langle 0|:\bar{U}_L U_R + \bar{U}_R U_L + \bar{D}_L D_R + \bar{D}_R D_L + \bar{S}_L S_R + \bar{S}_R S_L:|0\rangle\ \phi_\sigma + \\ &+ \sqrt{\frac{3}{2}}\kappa\langle 0|:\bar{D}_R S_L + D_L\bar{S}_R + \bar{D}_L S_R + D_R\bar{S}_L:|0\rangle\ \phi_h + \\ &+ \sqrt{\frac{3}{2}}\kappa\langle 0|:\cancel{\bar{D}_R S_L} + \cancel{D_L\bar{S}_R} - \cancel{\bar{D}_L S_R} - \cancel{D_R\bar{S}_L}:|0\rangle\ i\phi_k = \\ &= \theta\phi_\sigma + \omega\phi_h,\end{aligned}$$

where θ and ω were defined in eq. (4.4) and eq. (4.9). Now, we go back to the full one-loop effective potential which is composed of three elements that are to be discussed separately

$$V_{\text{eff}} = V_{\text{tree}} + V_{\text{CW}} + \Delta V(T). \tag{4.14}$$

The first term represents the tree-level field-dependent potential. From the potential energy terms in eq. (4.2), it can be shown that it bears the following form

$$\begin{aligned}V_{\text{tree}} = &\left(\frac{\lambda_1}{4}+\frac{\lambda_2}{4}\right)\phi_\sigma^4 + \left(\frac{\lambda_1}{4}+\frac{3\lambda_2}{8}\right)(\phi_h^4+\phi_k^4) - \frac{\Lambda_3}{3}\phi_\sigma^3 + \\ &+ \left(\frac{\lambda_1}{2}+\frac{3\lambda_2}{4}\right)\phi_h^2\phi_k^2 + \left(\frac{\lambda_1}{2}+\frac{3\lambda_2}{2}\right)\phi_h^2\phi_\sigma^2 + \left(\frac{\lambda_1}{2}+\frac{\lambda_2}{2}\right)\phi_k^2\phi_\sigma^2 + \\ &+ \frac{\Lambda_3}{2}(\phi_h^2-\phi_k^2)\phi_\sigma + \theta\phi_\sigma + \omega\phi_h.\end{aligned} \tag{4.15}$$

The CW contribution to the effective potential, given by eq. (2.2), could shift the VEVs and the physical masses even at zero temperatures. This poses a problem as we should not deviate from the experimentally measured value of the Higgs boson. The so-called *counterterms* are added to the potential to account for such shifts and match the results derived at tree-level [44]. The counterterm at $T = 0$, where $\phi_k = 0$, is rather straightforwardly given by the formula

$$V_{\text{ct}} = \delta\theta\ \phi_\sigma + \delta\omega\ \phi_h,$$

where $\delta\lambda_1$, $\delta\lambda_2$ and $\delta\Lambda_3$ have also been put to zero. To find the values of $\delta\theta$ and $\delta\omega$, we impose the following renormalization conditions

$$\left.\frac{\partial(V_{\text{CW}}+V_{\text{ct}})}{\partial\phi_\sigma}\right|_{\phi_\sigma,\phi_h} = \left.\frac{\partial(V_{\text{CW}}+V_{\text{ct}})}{\partial\phi_h}\right|_{\phi_\sigma,\phi_h} = 0$$

which directly result in

$$\delta\theta = -\frac{\partial V_{\rm CW}}{\partial \phi_\sigma}\bigg|_{\phi_\sigma,\phi_h} \qquad \text{and} \qquad \delta\omega = -\frac{\partial V_{\rm CW}}{\partial \phi_h}\bigg|_{\phi_\sigma,\phi_h}. \tag{4.16}$$

As before, we construct four 4×4 field-dependent mass-squared matrices which, upon numerical diagonalization, would give the field-dependent masses of 16 of the fields. As in Section 4.4, the two remaining degrees of freedom do not couple to any of the other fields and are obtained by differentiating twice with respect to the field in question. We examine the same four cases as in Section 4.4 and the Hessian mass-squared matrices, $M^2_{\rm NPS}$, $M^2_{\rm NS}$, $M^2_{\rm CPS}$ and $M^2_{\rm CS}$, are calculated, where N (C) in the subscripts stands for neutral (charged) and PS (S) stands for pseudoscalars (scalars). The entries of those matrices are given in Section C, where the thermal-loop corrections computed below are also included.

Now, in order to derive an expression for the final temperature-dependent potential term in eq. (4.14), let us firstly introduce the field-dependent fermion and gauge boson masses that give the highest contribution to the temperature-dependent potential among the rest of the elementary particles. These are

$$m^2_W(\phi_\alpha) = \frac{g^2_W}{4}(\phi^2_h + \phi^2_k) \qquad m^2_Z(\phi_\alpha) = \frac{g^2_W + g^2_1}{4}(\phi^2_h + \phi^2_k) \tag{4.17}$$

$$m^2_t(\phi_h) = \frac{Y^2_t \phi^2_h}{2} \qquad m^2_b(\phi_h) = \frac{Y^2_b \phi^2_h}{2} \qquad m^2_\tau(\phi_h) = \frac{Y^2_\tau \phi^2_h}{2}, \tag{4.18}$$

where g_W and g_1 are, as before, the $SU(2)_{\rm W}$ and $U(1)_{\rm Y}$ SM gauge couplings and Y_t, Y_b and Y_τ are the Higgs-Yukawa couplings of the top quark, bottom quark and the tau meson, respectively. Note that we have included the contribution from the ϕ_k field to the masses of the gauge bosons in eq. (4.17) [44]. On the other hand, in order to simplify the analysis, we have made the assumption that only $\mathcal{H}$ couples to the SM fermion fields. Using the values from eq. (2.3), the temperature-dependent potential, as given in the last term of eq. (2.5), is written out as

$$\begin{aligned}\Delta V(T) = \frac{T^2}{24}\Big\{ &\mathrm{Tr}[M^2_{\rm NPS}] + \mathrm{Tr}[M^2_{\rm NS}] + \mathrm{Tr}[M^2_{\rm CPS}] + \mathrm{Tr}[M^2_{\rm CS}] + \\ &+ 6\left(m^2_t + m^2_b\right) + 2m^2_\tau + 3\left(2m^2_W + m^2_Z\right)\Big\}.\end{aligned}$$

In the model that we consider in this thesis, the fields that obtain a VEV, ϕ_σ, ϕ_h and ϕ_k, are not accompanied by a corresponding μ value. This makes it more intricate to calculate the thermal corrections since methods similar to the ones used in [25], for example, are no longer applicable. The easiest way turns out to be to add those values by hand into the potential. This means that eq. (4.15) is transformed in the following way

$$V_{\rm tree} \to V_{\rm tree} + \frac{1}{2}(\mu^2_\sigma + c_\sigma T^2)\phi^2_\sigma + \frac{1}{2}(\mu^2_h + c_h T^2)\phi^2_h + \frac{1}{2}(\mu^2_k + c_k T^2)\phi^2_k.$$

Once the field-dependent Hessian matrix is constructed and evaluated at $\mu_\sigma = \mu_h = \mu_k = 0$, the parameters proportional to T^2 will appear at the corresponding places. Using the relation

$$c_{\sigma,h,k} = \frac{1}{T^2}\frac{\partial^2 \Delta V(T)}{\partial(\phi_{\sigma,h,k})^2}$$

the thermal-loop corrections are easily obtained to be

$$\begin{aligned}
c_\sigma &= \frac{10}{3}\lambda_1 + 6\lambda_2 \\
c_h &= \frac{1}{8}g_W^2 + \frac{1}{16}(g_W^2 + g_1^2) + \frac{1}{4}(Y_b^2 + Y_t^2) + \frac{1}{12}Y_\tau^2 + \frac{10}{3}\lambda_1 + 6\lambda_2 \\
c_k &= \frac{1}{8}g_W^2 + \frac{1}{16}(g_W^2 + g_1^2) + \frac{10}{3}\lambda_1 + 6\lambda_2.
\end{aligned} \tag{4.19}$$

5 Results and Discussion

5.1 Gravitational wave signals versus peak frequencies

The results in this section have been calculated using the `CosmoTransitions` `Python` package [45]. The operation of the software and implementation of the model are explained in Section D. In the figures below, the sensitivity curves of the LISA [27] and the proposed DECIGO [46, 47, 48, 49] and BBO [50, 51] interferometers are extracted from [29], [52, 47] and [53, 54], respectively. The `CosmoTransitions` implementations of various models, which served as guidelines for the implementation of the current model, as well as the `Jupyter Notebook` used to generate the plots presented in this section have been developed by my supervisors together with Felipe Freitas. The signal-to-noise ratio (SNR) calculations have been obtained using the on-line `PTPlot` tool [26].

The parameters that serve as an input are the four mass scales $M_{\eta'(0)}$, $M_{\sigma(0)}$, $M_{H(0)}$ and $M_{\pi(0)}$ before EW symmetry breaking as well as the parameter $\delta = \frac{v}{u}$, where the numerator is fixed to $v = 246.22\,\text{GeV}$ [28]. The quartic couplings λ_1, λ_2 and the dimensionful parameter Λ_3 are then expressed in terms of the input parameters as given in eq. (4.6), eq. (4.7) and eq. (4.8). One of the quantities to be studied is the order parameter which gives an estimate for the strength of the phase transition. We use the same definition as in [25], namely

$$\frac{\Delta v_n}{T_n} \gtrsim \eta, \quad \Delta v_n = \left|v(T_n + \delta T) - v(T_n - \delta T)\right|, \quad v(T) \equiv \sqrt{\sum_{\alpha=h,k} v_\alpha(T)^2} + v_\sigma(T), \tag{5.1}$$

where v_h and v_k are the VEVs the two Higgs doublets $\mathcal{H}$ and $\mathcal{K}$, v_σ is the VEV of the scalar EW singlet σ at a given temperature T, T_n is the nucleation temperature, $\delta T \ll T_n$ is a

small deviation from the nucleation temperature, Δv_n is the absolute value of the difference between the VEVs computed before and after the transition and η is a parameter larger than zero. A requirement in one-Higgs-doublet models for the production of FOPTs that would also give rise to detectable gravitational waves, is that $\eta \gtrsim 1$. As discussed and shown in [25], such a requirement is not a must in the case of THDM, since values as low as 0.1 could give data points in the range of LISA's sensitivity. In multi-scalar theories, however, the parameter α defined in eq. (2.11) is the quantity that better serves the role of an order parameter. Nevertheless, as can be seen on several of the scatter plots below (Figure 4 — Figure 7) where the color of the points is determined by the value of $\Delta v_n/T_n$, the data points which fall on or above the sensitivity curves of LISA, DECIGO and BBO, indeed have values larger than unity. Order parameters having values close to zero lie very far away from the detectable regions. We can see a very clear correlation between $\Delta v_n/T_n$ and α — they both increase with the strength of the phase transition. Additionally, we can also deduce from the figures that a smaller value of the β/H parameter would result in a stronger FOPT.

The plots are obtained in four steps which we below refer to as *phases*, differing only in the allowed ranges of the input mass scales. In all of these phases the ratio $\delta = \frac{v}{u}$ is kept between 0.1 and 0.3 so that u is allowed to take values in the approximate range $[0.821, 2.46]$ TeV. In order to be fully consistent with EW precision tests and to ensure a small enough splitting between a_0 and f, both contributing to the observed Higgs resonance, the δ parameter needs to be kept below ~ 0.08, as discussed in [17]. The smaller the δ value, the closer we are to the SM but, additionally, the more complicated it becomes to obtain FOPTs. Therefore, a proper phenomenological analysis needs to be included and such an analysis could serve as an extension to the current study. The figures that we show and discuss below are a result of a very first trial to studying gravitational waves production from FOPTs described by the composite Higgs model presented earlier.

Here and in the discussion below, all masses are in units of GeV. In Phase I, a wide range of mass scales is considered:

$$\left\{M_{\sigma(0)}, M_{\pi(0)}, M_{\eta'(0)}\right\} \in \left[50.0, 1000.0\right] \qquad M_{H(0)} \in \left[120.0, 130.0\right].$$

This produces a significant amount of points for most of which a strong FOPT is not realized and which are not in the scope of neither LISA, nor DECIGO and BBO (Figure 4). Since the masses are randomly generated in the specified ranges, it is very unlikely that a "good" point would be found. Therefore, once such a point is spotted in this large data set, the search is being refined. A point that lies on LISA's sensitivity curve is located and its input parameters are extracted. In the following Phase II, the mass range is significantly narrowed and a new run with the following values is created

$$\begin{aligned} M_{\sigma(0)} &\in \left[880.0, 920.0\right] & M_{\pi(0)} &\in \left[400.0, 450.0\right] \\ M_{\eta'(0)} &\in \left[470.0, 500.0\right] & M_{H(0)} &\in \left[120.0, 130.0\right]. \end{aligned} \tag{5.2}$$

This is done with the purpose of collecting more points in the interesting regions. As Figure 5 shows, this approach is quite successful as now many more strong phase transition points in the desirable regions are found. One can see how for the mass range given in eq. (5.2) the data points with an order parameter of roughly unity form a very prominent line which then widens and stronger phase transitions are within the reach of the interferometers. Some weak phase transitions have also been generated but their number is significantly smaller compared to Figure 4.

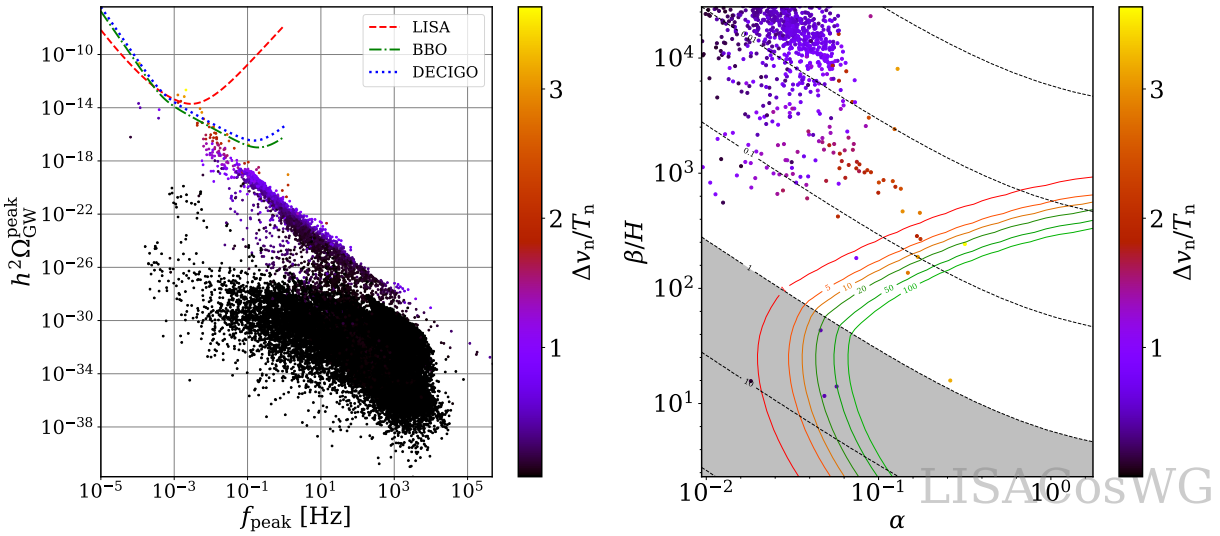

Figure 4: A scatter plot of the data points obtained during Phase I. *Left panel*: The peak value of the gravitational wave signal is plotted against the peak frequency where the color of the points is determined by the strength of the phase transition from eq. (5.1). In this and the following figures, the dashed, dotted and dashdotted lines represent the sensitivity curves of the LISA interferometer as well as the proposed DECIGO and BBO missions, respectively. In this very wide range of masses, it is difficult to generate points that would come close to the sensitivity curves. *Right panel:* A `PTPlot` of the nucleation rate parameter, β/H, against the strength of the phase transition, α. The diagonal dashed lines represent the ratio of the Hubble time to the fluid turnover time. The colored curved lines represent LISA's SNR (sensitivity curve and duration). The grey shaded regions shows the area where the sound wave source lasts longer than a Hubble time [55]. The shaded and unshaded regions make use of different formulae all given in [26]. From the plot, we notice a correlation between the strength of the phase transition and the order parameter. The points with a larger value of $\Delta v_n/T_n$ "spill" towards the detectable regions.

What draws the attention in eq. (5.2) is that the π pseudo-Goldstone state is found to have a mass as large as 400 GeV. This is rather unusual but should not be excluded as a possible scenario. Moreover, when refining the search in Phase II, such that we are close to LISA's sensitivity, only a single point was taken into account. Therefore, in a third and a fourth set of points, we consider a broader mass range but again restrict the

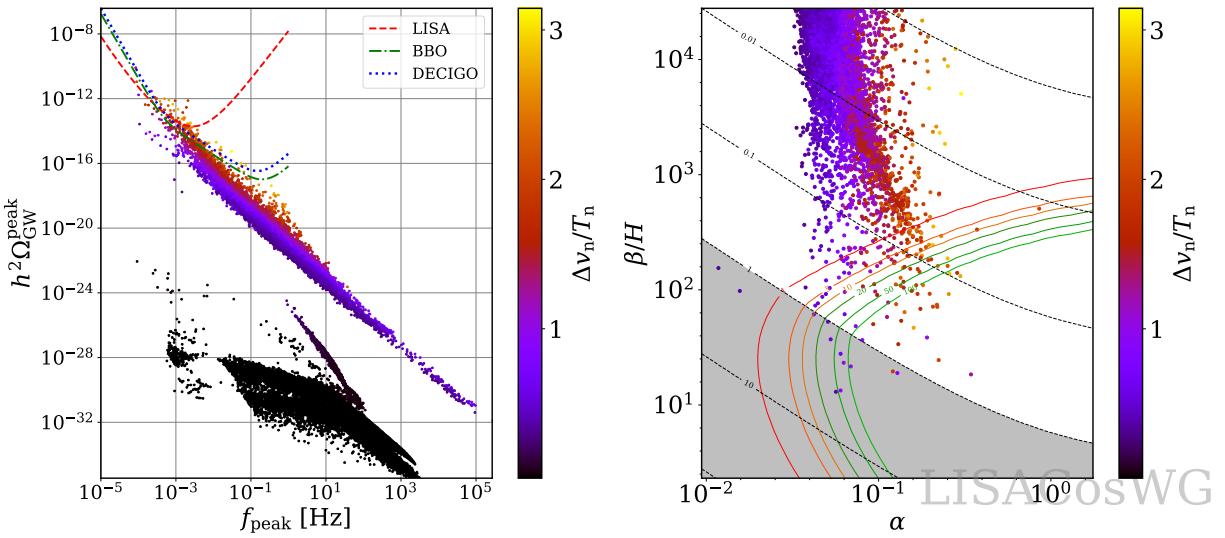

Figure 5: A scatter plot of the data points obtained during Phase I. *Left panel*: The peak value of the gravitational wave signal is plotted against the peak frequency where the color of the points is determined by the strength of the phase transition from eq. (5.1). *Right panel:* A `PTPlot` of the nucleation rate parameter, β/H, against the strength of the phase transition, α.

input values in such a way that the expected output lies in the vicinity of the sensitivity curves. Here, we introduce the two remaining phases: Phase III, where a light pion mass is considered ($50\,\text{GeV} \leq M_{\pi(0)} \leq 125\,\text{GeV}$) and Phase IV, where we examine a heavier pion mass ($125\,\text{GeV} \leq M_{\pi(0)} \leq 500\,\text{GeV}$) with the rest of the masses taking values in the following intervals

$$M_{\sigma(0)} \in \big[840.0, 990.0\big] \qquad M_{\eta'(0)} \in \big[400.0, 550.0\big] \qquad M_{H(0)} \in \big[120.0, 130.0\big].$$

The results are shown in Figure 6 and Figure 7.

Quite an interesting feature of Figure 6 is that a certain region of the graph is very scarcely populated — the majority of the transitions are either very strong or very weak. In Phase IV, on the other hand, we find numerous data points scattered in this region having an order parameter somewhat below unity. This is not entirely surprising as a wider range of values is considered in Phase IV.

What we can further ask is which VEV shift contributes the most to the phase transitions. For that, let us compare the VEVs $\{v_\sigma, v_h, v_k\}$ of the classical background fields $\{\phi_\sigma, \phi_h, \phi_k\}$ at finite temperatures. We choose to display the points from Phase II as the difference in the VEVs is most clearly seen. The conclusion from this paragraph would be the same regardless of which Phase we choose to work with. The results are shown in Figure 8. The color of the scattered plot is determined by the value of the VEVs just before the phase transition when $T = T_n + \delta T$ (left panels) and right after the phase transitions when

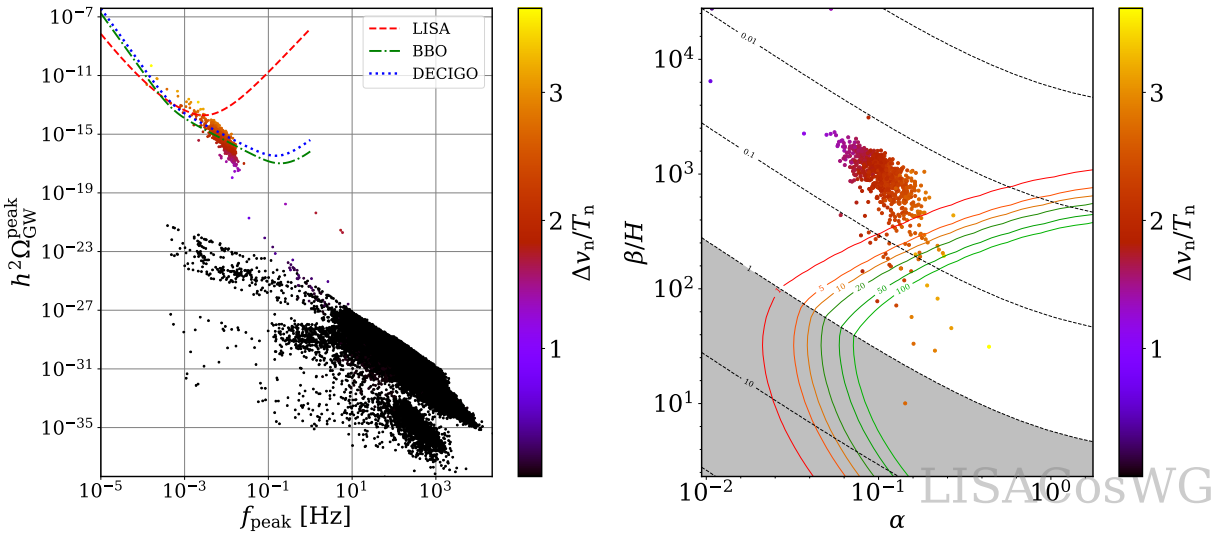

Figure 6: A scatter plot of the data points obtained during Phase III. *Left panel*: The peak value of the gravitational wave signal is plotted against the peak frequency where the color of the points is determined by the strength of the phase transition from eq. (5.1). *Right panel:* A `PTPlot` of the nucleation rate parameter, β/H, against the strength of the phase transition, α.

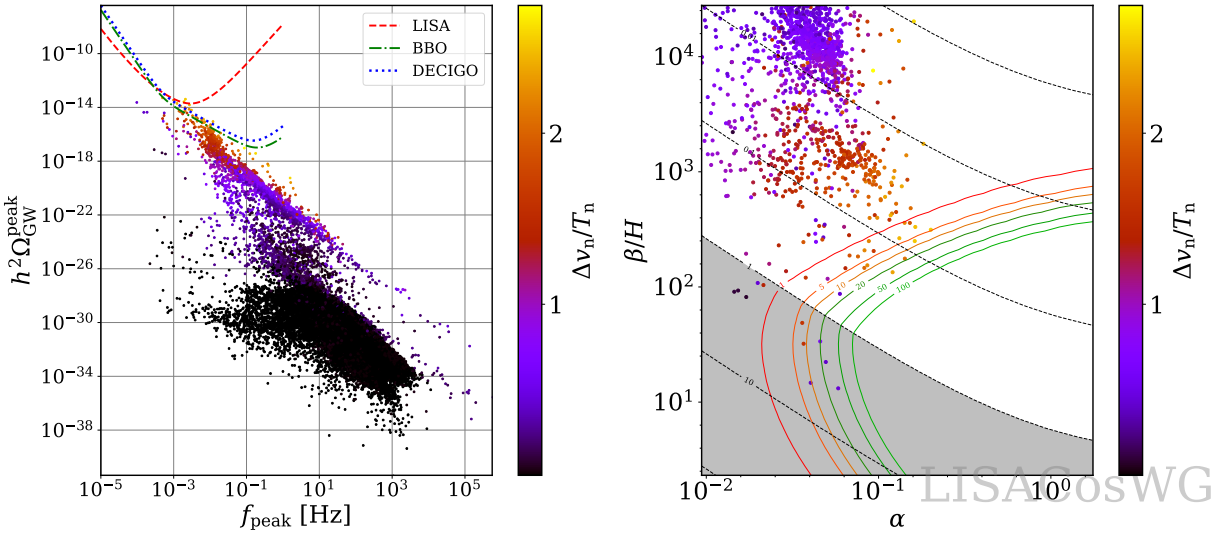

Figure 7: A scatter plot of the data points obtained during Phase IV. *Left panel*: The peak value of the gravitational wave signal is plotted against the peak frequency where the color of the points is determined by the strength of the phase transition from eq. (5.1). *Right panel:* A `PTPlot` of the nucleation rate parameter, β/H, against the strength of the phase transition, α.

$T = T_n - \delta T$ (right panels). The subscripts i and f stand for *initial* and *final*. The first pair of plots suggests that the initial VEV of the ϕ_σ field undergoes barely any change as the color of the points between the left and the right plots is almost unaffected. The third pair of plots on the same figure lead to a similar conclusion. Here, however, the VEV of the $\mathcal{K}$ Higgs doublet is almost zero both before and after the phase transition. The second pair of plots, on the other hand, shows that the initial and final VEVs of the $\mathcal{H}$ Higgs doublet affects the transition the most. Even though there is a slight shift in scales between the left and the right plot, the VEV of the points before the transition that lie close to the sensitivity curves of the three interferometers is $\sim 50\,\text{GeV}$, whereas the same points obtain a value of $\sim 250\,\text{GeV}$ after the transition. We also note that no significant VEV change is seen for most of the weaker phase transitions falling below the sensitivity curves.

5.2 Benchmark points

While points above the sensitivity curves are ones that are in the observable region of the interferometers, this does not necessarily mean that the signal would be observed. What a possible observation also depends on are details such as detector configuration, exposure time, source modeling and details of the noise model. In order to give a qualitative estimation of the extent to which a certain scenario can be reconstructed with the LISA interferometer, the SNR of the observation is estimated [56, 57]. As discussed in [25], we can take the "optimistic" approach of SNR ≥ 10 in which case all eight points from Table 1 and Table 2 could be observed already after three years. We can also take the more "conservative" approach where we require the points to have an SNR ≥ 50. In that case, some of the points fail to be within LISA's range even after an exposure time of seven years. The parameters of the last four points, however, produce an SNR value well above 50 already after three years.

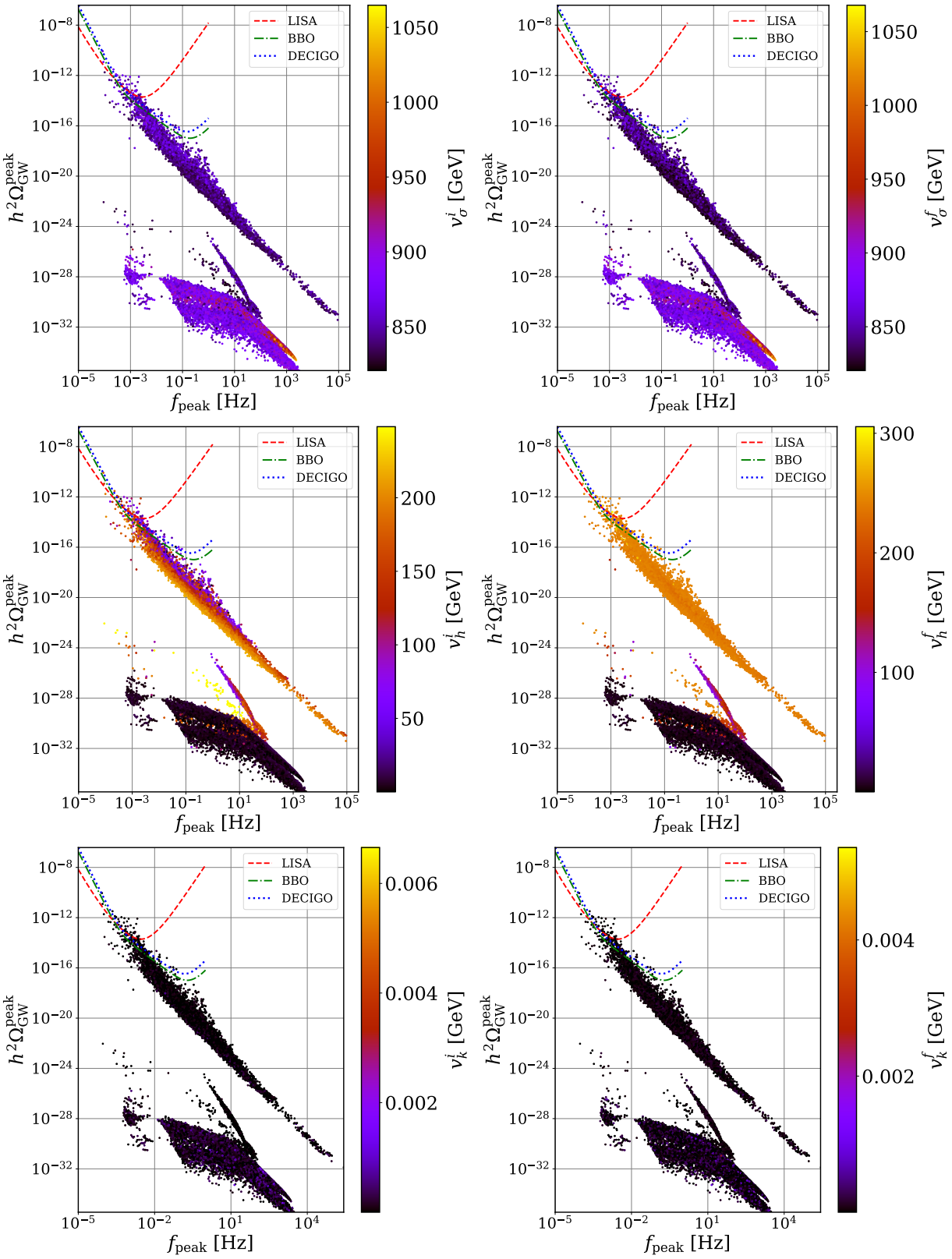

Figure 8: A scatter plot of the data points obtained during Phase II. *Left panel*: The peak value of the gravitational wave signal is plotted against the peak frequency where the color of the points is determined by the value of v_s^i, v_h^i or v_k^i. *Right panel:* The peak value of the gravitational wave signal is plotted against the peak frequency where the color of the points is determined by the value of v_s^f, v_h^f or v_k^f.

Table 1: Eight benchmark points around and above the sensitivity curve of LISA. Given are the values for the nucleation temperature (in GeV), the parameter defined in eq. (5.1), the phase transition strength, the nucleation rate parameter as well as the initial and final values of the σ, h and k VEVs (in GeV).

id	T_n	Δv_n	α	β/H	v_σ^i	v_σ^f	v_h^i	v_h^f	v_k^i	v_k^f
1	86.0	232	0.1719	359	1481	1435	229	506	-0.0000186	0.000014
2	69.0	217	0.2715	437	1424	1378	235	497	-0.0000185	0.000138
3	89.0	247	0.1928	253	1456	1406	220	516	0.0000083	0.000252
4	130	414	0.1638	199	1515	1457	88	560	0.0000102	0.000026
5	122	285	0.1267	72.0	1408	1355	170	509	0.000227	0.000484
6	83.0	241	0.2124	29.0	1197	1147	144	435	0.000007	0.000218
7	124	336	0.1569	33.2	1464	1405	149	543	0.000004	-0.000032
8	55.6	203	0.4375	31.2	1449	1406	242	487	-0.000002	0.000030

Table 2: Eight benchmark points around and above the sensitivity curve of LISA. Given are the values for the σ, π, η' and H masses, the peak frequency (in Hz), the value of the gravitational wave signal as well as the SNR values for three and for seven years.

id	$M_{\sigma(0)}$	$M_{\pi(0)}$	$M_{\eta'(0)}$	$M_{H(0)}$	f_{peak}	$h^2\Omega_{\text{GW}}^{\text{peak}}$	SNR: 3 years	SNR: 7 years
1	988	94.0	480	125	0.002919	$1.384 \cdot 10^{-14}$	14	22
2	971	70.0	418	122	0.002832	$4.809 \cdot 10^{-14}$	29	45
3	983	68.0	428	122	0.002123	$3.557 \cdot 10^{-14}$	37	57
4	974	124	546	127	0.002453	$4.669 \cdot 10^{-14}$	42	64
5	944	87.0	463	126	0.000824	$8.556 \cdot 10^{-14}$	62	95
6	849	117	414	130	0.000218	$5.496 \cdot 10^{-12}$	122	187
7	962	59	473	128	0.000388	$1.083 \cdot 10^{-12}$	144	219
8	968	69.2	475	127	0.000164	$4.273 \cdot 10^{-11}$	232	355

6 Conclusion

In a thesis written by Jacob Taxén several years back [17], phenomenological implications of the composite Higgs model presented above have been studied and it has been demonstrated that present-day colliders do not have the power to resolve the double-peak of the Higgs. Nevertheless, novel methods that could probe the theory under consideration have been developed, namely detection of gravitational waves from the process of early-Universe bubble nucleation. In the present thesis, we have extended the study by Jacob and have discussed possible cosmological implications of the model.

In the previous sections, a model based on a strongly coupled $SU(3)_{\text{TC}}$ sector has been introduced, where T-quarks are confined at energy scales $\Lambda_{\text{TC}} \sim \mathcal{O}(\text{TeV})$. We have discussed a possible way to explain the Higgs boson as a composite hadron-like object that may originate from a QCD-like confined sector at high energies. As the SM does not feature the existence of strong FOPTs, we have analysed the characteristics of phase transitions in this composite Higgs scenario and looked at the possibility to generate potentially observable primordial gravitational wave spectra. The latter could help setting more stringent bounds on the parameter space of the model when combined with collider constraints. Such an analysis is planned for future studies.

Implementing the model in `CosmoTransitions` made the search for such FOPTs possible. As expected, the majority of the events turned out to be too weak and, therefore, too far away from the sensitivity curves of LISA, BBO and DECIGO. Nevertheless, after a larger set of data points was obtained, a number of strong FOPTs showed up on the plots. In the current data set, only a single point was found to exhibit a strong enough phase transition such that it overlaps with LISA's sensitivity curve on the `PTPlot`. Nevertheless, a larger data set might lead to discovering many more points lying in the desirable regions.

The cosmological implications of such QCD-like composite Higgs TC models could be extended in many ways. An additional degree of freedom could be given a non-zero VEV, which implies a larger number of possible transitions. It might also affect the effective potential in such a way that the strength of the phase transitions is amplified. These results could also be compared to the cosmological parameters of other models.

Models like the one considered here are indeed very promising and their properties should further be studied. Here, we have mainly considered LISA's contribution to the gravitational wave signal. However, a significant number of points fell well above the sensitivity curves of BBO and DECIGO. The future of such state-of-the art interferometers looks very bright and so does the study of gravitational wave signals from FOPTs. It is exciting to see what lies ahead.

7 Acknowledgements

Not a few people made this thesis possible. I would firstly like to thank my supervisor Roman Pasechnik for the help, guidance and patience throughout this project. I would like to thank António Morais for the valuable comments on the model. I would again like to thank Roman Pasechnik, António Morais as well as Felipe Freatis for providing the example codes that I could use and adapt to the model in this thesis. I am very thankful to Malin Sjödahl for the discussions regarding the process of thesis writing and also for providing a home licence for the `Mathematica` software very quickly. I would like to thank Christian Bierlich for always giving fast and helpful responses regarding all technical issues that I encountered. I am extremely grateful to Danislav Kirov without whose support, positivity and computer knowledge everything would have seemed impossible. Lastly, I am ever so grateful to my mom, dad and sister for their absolutely endless support.

Appendices

A Electroweak phase transition

The zero-temperature tree-level scalar potential bears the following quartic form:

$$V_{\text{tree}}(\varphi) = \lambda\left(\varphi^2 - v_{\text{EW}}^2\right)^2,$$

where φ is the Higgs field, λ is the Higgs self-coupling constant and $v_{\text{EW}} = \langle\varphi\rangle_{T=0}$ is the Higgs VEV obtained by applying a minimization condition on the potential with respect to φ. The temperature contribution that is to be added to $V_{\text{tree}}(\varphi)$ comes from the pressure term, $(-p_i)$, exerted by an (anti-)particle i in the medium that couples to the SM Higgs. It bears the form

$$\sum_i(-p_i) = -\frac{1}{6\pi^2}\sum_i g_i \int_0^\infty \frac{k^4\ dk}{\sqrt{k^2+m_i^2}} \frac{1}{e^{\frac{\sqrt{k^2+m_i^2}}{T}} \mp 1},$$

where k is the four-momentum of the particle, g_i is the number of spin states, m_i is the respective mass and the minus/plus sign corresponds to bosons/fermions. Below, the sum over i is implied. We normalize the expression to the temperature by defining the quantities

$$x = \frac{k}{T} \Rightarrow dk = T dx \qquad z_i = \frac{m_i}{T}$$

and rewrite $(-p_i)$ in the form

$$\begin{aligned} -p_i &= -\frac{g_i}{6\pi^2}\int_0^\infty \frac{x^4 \cancel{T^4}\ \cancel{T}\ dx}{\sqrt{x^2\cancel{T^2} + z_i^2\cancel{T^2}}} \frac{1}{e^{\frac{\sqrt{x^2\cancel{T^2}+z_i^2\cancel{T^2}}}{\cancel{T}}} \mp 1} = \\ &= -\frac{g_i T^4}{6\pi^2}\int_0^\infty \frac{x^4\ dx}{\sqrt{x^2+z_i^2}} \frac{1}{e^{\sqrt{x^2+z_i^2}} \mp 1} = \\ &= -\frac{g_i T^4}{6\pi^2} I(z_i^2). \end{aligned} \tag{A.1}$$

In order to solve the integral $I(z_i^2)$, we take the limit $T \gg m_i \Rightarrow T \gg z_i T \Rightarrow z_i^2 \ll 1$. This would correspond to pressure being only exerted by photons and light fermions. We then

perform a Taylor expansion with respect to z_i^2 up to first order

$$
\begin{aligned}
I(z_i^2) &\approx \cancel{I(z_i^2)\Big|_{z_i^2=0}} + z_i^2 \left(\frac{dI}{dz_i^2}\right)\Big|_{z_i^2=0} + \text{H.O.} \approx \\
&\approx z_i^2 \int_0^\infty \frac{d}{dz_i^2}\left(\frac{x^4\, dx}{\sqrt{x^2+z_i^2}}\frac{1}{e^{\sqrt{x^2+z_i^2}}\mp 1}\right)\Big|_{z_i^2=0} = \\
&= z_i^2 \int_0^\infty \left(-\frac{1}{2}\frac{x^4 dx}{(x^2+z_i^2)^{3/2}}\frac{1}{e^{\sqrt{x^2+z_i^2}}\mp 1} - \frac{x^4 dx}{\sqrt{x^2+z_i^2}}\frac{e^{\sqrt{x^2+z_i^2}}}{2\left(e^{\sqrt{x^2+z_i^2}}\mp 1\right)^2\sqrt{x^2+z_i^2}}\right)\Big|_{z_i^2=0} = \\
&= -\frac{z_i^2}{2}\left(\int_0^\infty \frac{x dx}{e^x\mp 1} + \int_0^\infty \frac{x^2 e^x dx}{(e^x\mp 1)^2}\right) = -\frac{z_i^2}{2}\left(I'_\mp(x) + I''_\mp(x)\right), \qquad \text{(A.2)}
\end{aligned}
$$

where the zeroth order term has been omitted as it corresponds to pressure due to massless particles. For the first integral, $I'_\mp(x)$, we can use the relations

$$\int_0^\infty \frac{x^{n-1}}{e^x-1}dx = \Gamma(n)\zeta(n) \qquad \int_0^\infty \frac{x^{n-1}}{e^x+1}dx = (1-2^{1-n})\Gamma(n)\zeta(n)$$

for $n=2$, $\zeta(2)=\frac{\pi^2}{6}$ and $\Gamma(2)=1$. Therefore

$$I'_-(x) = \int_0^\infty \frac{x}{e^x-1}dx = \frac{\pi^2}{6} \qquad I'_+(x) = \int_0^\infty \frac{x}{e^x+1}dx = \frac{\pi^2}{12}.$$

The second integral, $I''_\mp(x)$, can be evaluated through integration by parts

$$I''_\mp(x) = \int_0^\infty \frac{x^2 e^x}{(e^x\mp 1)^2}dx = \cancel{\left[-\frac{x^2}{e^x\mp 1}\right]_0^{\infty}}^{0} + 2\int_0^\infty \frac{x}{e^x\mp 1}dx = 2I'_\mp(x).$$

Therefore

$$I''_-(x) = \int_0^\infty \frac{x}{e^x-1}dx = \frac{\pi^2}{3} \qquad I''_+(x) = \int_0^\infty \frac{x}{e^x+1}dx = \frac{\pi^2}{6}.$$

Using the numerical results for the primed integrals and summing over the boson (minus sign) and fermion (plus sign), we rewrite eq. (A.2) in the following form

$$
\begin{aligned}
I(z_i^2) &= -\frac{z_i^2}{2}\left[\left(\frac{\pi^2}{6}+\frac{\pi^2}{3}\right)_{\text{bosons}} + \left(\frac{\pi^2}{12}+\frac{\pi^2}{6}\right)_{\text{fermions}}\right] = \\
&= -\frac{z_i^2}{2}\left[\left(\frac{\pi^2}{2}\right)_{\text{bosons}} + \left(\frac{\pi^2}{4}\right)_{\text{fermions}}\right].
\end{aligned}
$$

Plugging in the result into eq. (A.1), we obtain

$$-p_i = \frac{g_i T^2}{6\cancel{\pi^2}} \frac{m_i^2}{2} \left[\left(\frac{\cancel{\pi^2}}{2} \right)_{\text{bosons}} + \left(\frac{\cancel{\pi^2}}{4} \right)_{\text{fermions}} \right]$$

$$-p_i = \frac{T^2}{24} \left[\sum_{\text{bosons}} g_i h_i^2 \varphi^2 + \frac{1}{2} \sum_{\text{fermions}} g_i h_i^2 \varphi^2 \right],$$

where in the second equation we expressed the mass as, according to the SM, being proportional to the field φ with a mass proportionality constant h_i. The relevant particles that couple to the Higgs most strongly are given in Table 3 with their respective value of h_i.

Table 3: A list of the masses and mass proportionality constants of the SM fermions and bosons that couple most strongly to the Higgs field. Here, Y_t Y_b and Y_τ are the Higgs-Yukawa coupling of the top quark, the bottom quark and the τ meson, λ is the Higgs self-coupling, and g_W and g_1 are the gauge couplings of the W_μ^a and B_μ bosons [58].

Particle	Mass [GeV] [28]	h_i
t	172.76 ± 0.30	Y_t
b	$4.18^{+0.03}_{-0.02}$	Y_b
τ	1.77686 ± 0.00012	Y_τ
H	125.25 ± 0.17	$\sqrt{2\lambda}$
$W^\pm$	80.379 ± 0.012	$\frac{g_W}{\sqrt{2}}$
Z	91.1876 ± 0.0021	$\frac{\sqrt{g_W^2+g_1^2}}{\sqrt{2}}$

B The Hubble Time

We begin this section by taking for granted the equation relating density, ρ, and pressure, p, when the matter in the Universe is in thermal equilibrium and at zero chemical potential:

$$\frac{d\rho}{p+\rho} = -3\ d(\ln a), \tag{B.1}$$

where $a(t)$ is a scale factor that grows with time as the Universe expands. In terms of this factor, the Hubble parameter is defined as

$$H \equiv \frac{\dot{a}}{a}. \tag{B.2}$$

In the very early Universe, the energy density is primarily due to relativistic matter, which gives the following equation of state

$$p = \frac{1}{3}\rho. \tag{B.3}$$

Plugging in eq. (B.3) into eq. (B.1), one obtains the following expressions:

$$\frac{d\rho}{\rho} = -4\frac{da}{a} \quad \Leftrightarrow \quad d(\ln\rho) = d(-4\ln a) \quad \Leftrightarrow \quad d(\ln\rho) = d(\ln a^{-4})$$

$$\Rightarrow \rho \propto \frac{1}{a^4}.$$

We can now use the Friedmann equation for a spatially flat Universe, which relates the Hubble parameter to the total energy density, to express the scale factor as a function of time

$$\left(\frac{\dot{a}}{a}\right)^2 = \frac{8\pi}{3}G\rho, \tag{B.4}$$

where G is the gravitational constant. Then

$$\left(\frac{\dot{a}}{a}\right)^2 \propto \frac{1}{a^4} \quad \Leftrightarrow \quad \frac{da}{dt} \propto a^{-1}.$$

Let us make the following ansatz

$$a(t) \propto t^{\gamma}$$

and solve the last equation for γ

$$\frac{d(t^{\gamma})}{dt} \propto t^{-\gamma} \quad \Leftrightarrow \quad \gamma t^{\gamma-1} \propto t^{-\gamma} \quad \Leftrightarrow \quad \gamma - 1 = -\gamma \quad \Leftrightarrow \quad \gamma = \frac{1}{2}.$$

We have therefore found that $a(t)$ bears the form

$$a(t) \propto t^{1/2}.$$

Now, going back to eq. (B.2), the following relation is obtained

$$H = \frac{1}{2}\frac{t^{-1/2}}{t^{1/2}} = \frac{1}{2t} \quad \Leftrightarrow \quad t = \frac{1}{2H},$$

where t we call the *Hubble time*. It is a measure of the age of the Universe at a particular time, given that the Universe has been expanding uniformly.

Derivations of eq. (B.1), eq. (B.3) and eq. (B.4) can be found for example in [23].

C Entries of the field-dependent mass-squared Hessian matrices

Let us for convenience define the quantity:

$$\phi_{\rm all}^2 = \phi_\sigma^2 + \phi_h^2 + \phi_k^2.$$

The entries of the field-dependent mass-squared Hessian matrices are given below.

1. Neutral pseudoscalar T-mesons

$$M^2_{\rm NPS,11} = 2\left[\lambda_1\phi_{\rm all}^2 + \lambda_2(\phi_{\rm all}^2 + 2\phi_k^2) + 2\Lambda_3\phi_\sigma\right]$$

$$M^2_{\rm NPS,22} = 2\lambda_1(\phi_{\rm all}^2 + 2\phi_k^2) + \lambda_2(2\phi_\sigma^2 + 3\phi_h^2 + 9\phi_k^2) - 2\Lambda_3\phi_\sigma^2 + 2c_kT^2$$

$$M^2_{\rm NPS,33} = 2\lambda_1\phi_{\rm all}^2 + \lambda_2(7\phi_h^2 + 3\phi_k^2 + 2\phi_\sigma^2) - 2\Lambda_3$$

$$M^2_{\rm NPS,44} = 2\lambda_1\phi_{\rm all}^2 + \lambda_2(3\phi_h^2 + 3\phi_k^2 + 2\phi_\sigma^2) - 2\Lambda_3\phi_\sigma^2$$

$$M^2_{\rm NPS,55} = M_\xi^2 = 6\lambda_2^2\phi_\sigma^2 + 2\Lambda_3\phi_\sigma + 3\lambda_2(\phi_h^2 + 3\phi_k^2) + 2\lambda_1\phi_{\rm all}^2 + 2c_kT^2$$

$$M^2_{\rm NPS,12} = -2\phi_h(\Lambda_3 - 2\lambda_2\phi_\sigma)$$

$$M^2_{\rm NPS,13} = -\frac{\lambda_2(\phi_h^2 + 3\phi_k^2)}{\sqrt{2}}$$

$$M^2_{\rm NPS,14} = -\sqrt{\frac{3}{2}}\lambda_2(\phi_h^2 + 3\phi_k^2)$$

$$M^2_{\rm NPS,23} = -\sqrt{2}\phi_h(\Lambda_3 + \lambda_2\phi_\sigma)$$

$$M^2_{\rm NPS,24} = -\sqrt{6}\phi_h(\Lambda_3 + \lambda_2\phi_\sigma)$$

$$M^2_{\rm NPS,34} = -2\sqrt{3}\lambda_2\phi_h^2$$

2. Neutral scalar T-mesons

$$M^2_{\mathrm{NS},11} = 2\left[c_\sigma T^2 + \lambda_1(\phi^2_{\mathrm{all}} + 2\phi^2_\sigma) + \lambda_2(3\phi^2_\sigma + 3\phi^2_h + \phi^2_k) - 2\Lambda_3\phi_\sigma\right]$$

$$M^2_{\mathrm{NS},22} = 2c_h T^2 + 2\lambda_1(\phi^2_{\mathrm{all}} + 2\phi^2_h) + 3\lambda_2(2\phi^2_\sigma + 3\phi^2_h + \phi^2_k) + 2\Lambda_3\phi_\sigma$$

$$M^2_{\mathrm{NS},33} = 2\lambda_1\phi^2_{\mathrm{all}} + 3\lambda_2(\phi^2_{\mathrm{all}} + \phi^2_\sigma) + 2\Lambda_3\phi_\sigma$$

$$M^2_{\mathrm{NS},44} = 2\lambda_1\phi^2_{\mathrm{all}} + \lambda_2(3\phi^2_h + 7\phi^2_k + 6\phi^2_\sigma) + 2\Lambda_3\phi^2_\sigma$$

$$M^2_{\mathrm{NS},55} = M^2_g = 2\lambda_2^2\phi^2_\sigma - 2\Lambda_3\phi_\sigma + 3\lambda_2(3\phi^2_h + \phi^2_k) + 2\lambda_1\phi^2_{\mathrm{all}} + 2c_h$$

$$M^2_{\mathrm{NS},12} = 2\phi_h\left[2(\lambda_1 + 3\lambda_2)\phi_\sigma + \Lambda_3\right]$$

$$M^2_{\mathrm{NS},13} = -\sqrt{\frac{3}{2}}\lambda_2(3\phi^2_h + \phi^2_k)$$

$$M^2_{\mathrm{NS},14} = -\frac{\lambda_2(3\phi^2_h + \phi^2_k)}{\sqrt{2}}$$

$$M^2_{\mathrm{NS},23} = \sqrt{6}\phi_h(\Lambda_3 - 3\lambda_2\phi_\sigma)$$

$$M^2_{\mathrm{NS},24} = \sqrt{2}\phi_h(\Lambda_3 - 3\lambda_2\phi_\sigma)$$

$$M^2_{\mathrm{NS},34} = -2\sqrt{3}\lambda_2\phi^2_k$$

3. Charged (pseudo)scalar T-mesons

$$M^2_{\mathrm{C(P)S},11} = M^2_{\mathrm{C(P)S},22} = M^2_{\mathrm{C(P)S},33} = M^2_{\mathrm{C(P)S},44} = 2\lambda_1\phi^2_{\mathrm{all}} + \lambda_2(4\phi^2_\sigma + 3\phi^2_h + 3\phi^2_k)$$

$$M^2_{\mathrm{C(P)S},12} = M^2_{\mathrm{C(P)S},34} = \mp 2\phi_\sigma(\Lambda_3 + \lambda_2\phi_\sigma)$$

$$M^2_{\mathrm{C(P)S},13} = M^2_{\mathrm{C(P)S},24} = 2\sqrt{6}\lambda_2\phi_h\phi_\sigma$$

$$M^2_{\mathrm{C(P)S},14} = M^2_{\mathrm{C(P)S},23} = \sqrt{6}\phi_h(\pm\Lambda_3 \mp \lambda_2\phi_\sigma)$$

where the upper (lower) sign corresponds to pseudoscalars (scalars).

D CosmoTransitions

`CosmoTransitions` [45] is a `Python` package which makes it possible to numerically compute the cosmological parameters from Section 2.3 and model-dependent cosmological phase transitions at finite-temperatures. As explained in [45], there are three main parts that need to be implemented.

The first task is implementing the model which is mainly done in the `generic_potential` class. We introduce the masses of the heaviest of the elementary particles, whose contribution to the thermal correction is the biggest — the top, the bottom and the tau, together with the mass and VEV of the Higgs. The input parameters are four of the mass scales — $M^2_{\eta'(0)}$, $M^2_{\sigma(0)}$, $M^2_{\pi(0)}$ and $M^2_{H(0)}$ with the help of which one can express the three constants that enter the Lagrangian, λ_1, λ_2 and Λ_3 as well as the quark condensates.

The following parameters should be present in the initialization method:

- the parameters λ_1, λ_2 and Λ_3 given by eq. (4.6), eq. (4.7) and eq. (4.8), respectively;
- the tadpole equations given by eq. (4.12) and eq. (4.13);
- the Yukawa couplings given by

$$Y_t = \frac{\sqrt{2}\, m_t}{v} \qquad Y_b = \frac{\sqrt{2}\, m_b}{v} \qquad Y_\tau = \frac{\sqrt{2}\, m_\tau}{v},$$

  where m_t, m_b and m_τ are the masses of the top and bottom quarks and the tau meson, respectively;
- the masses-squared of the $W^\pm$ and Z bosons from eq. (4.17) as well as the masses-squared of the τ, the bottom and the top from eq. (4.18);
- the thermal loop corrections given by eq. (4.19);
- the counterterms given by eq. (4.16);

Next, we need to specify the physical regions by imposing the following tree-level conditions:

$$|\lambda_1| < 4\pi; \qquad |\lambda_2| < 4\pi; \qquad \left|\frac{\Lambda_3}{u}\right| < 4\pi.$$

Two other methods are dedicated to the implementation of the tree-level potential from eq. (4.15) as well as the mass-squared matrices whose entries are given in Section C.

References

[1] D. Tong, "Quantum Fields: The Real Building Blocks of the Universe." https://youtu.be/zNVQfWC_evg.

[2] "The Royal Institution." https://www.rigb.org/.

[3] **ATLAS** Collaboration, G. Aad *et al.*, "Observation of a new particle in the search for the Standard Model Higgs boson with the ATLAS detector at the LHC," *Phys. Lett. B* **716** (2012) 1–29, arXiv:1207.7214 [hep-ex].

[4] **CMS** Collaboration, S. Chatrchyan *et al.*, "Observation of a New Boson at a Mass of 125 GeV with the CMS Experiment at the LHC," *Phys. Lett. B* **716** (2012) 30–61, arXiv:1207.7235 [hep-ex].

[5] L. Susskind, "Dynamics of Spontaneous Symmetry Breaking in the Weinberg-Salam Theory," *Phys. Rev. D* **20** (1979) 2619–2625.

[6] C. Grojean, "Beyond the standard Higgs after the 125 GeV Higgs discovery," *Phil. Trans. Roy. Soc. Lond. A* **373** no. 2032, (2014) 20140042.

[7] H. Georgi, H. R. Quinn, and S. Weinberg, "Hierarchy of Interactions in Unified Gauge Theories," *Phys. Rev. Lett.* **33** (1974) 451–454.

[8] A. Maciel, "Hierarchy and BSM." http://www.cbpf.br/~maciel/evjas/a08_hierarchy.pdf.

[9] A. D. Sakharov, "Violation of CP Invariance, C asymmetry, and baryon asymmetry of the universe," *Sov. Phys. Usp.* **34** no. 5, (1991) 392–393.

[10] N. S. Manton, "Topology in the Weinberg-Salam Theory," *Phys. Rev. D* **28** (1983) 2019.

[11] F. R. Klinkhamer and N. S. Manton, "A Saddle Point Solution in the Weinberg-Salam Theory," *Phys. Rev. D* **30** (1984) 2212.

[12] P. B. Arnold and L. D. McLerran, "Sphalerons, Small Fluctuations and Baryon Number Violation in Electroweak Theory," *Phys. Rev. D* **36** (1987) 581.

[13] N. S. Manton, "The Inevitability of Sphalerons in Field Theory," *Phil. Trans. Roy. Soc. Lond. A* **377** no. 2161, (2019) 20180327, arXiv:1903.11573 [hep-th].

[14] K. Kajantie, M. Laine, K. Rummukainen, and M. E. Shaposhnikov, "Is there a hot electroweak phase transition at m(H) larger or equal to m(W)?," *Phys. Rev. Lett.* **77** (1996) 2887–2890, arXiv:hep-ph/9605288.

[15] A. Degee, "Higgs mechanism in the general Two-Higgs-Doublet Model,". http://hdl.handle.net/2268/68445.

[16] O. Witzel, "Review on Composite Higgs Models," *PoS* **LATTICE2018** (2019) 006, arXiv:1901.08216 [hep-lat].

[17] J. Taxén, "Chirally Symmetric Technicolor Model: A possible origin of the Higgs Boson,". http://lup.lub.lu.se/student-papers/record/7762446.

[18] L. Susskind, "THE GAUGE HIERARCHY PROBLEM, TECHNICOLOR, SUPERSYMMETRY, AND ALL THAT.," *Phys. Rept.* **104** (1984) 181–193.

[19] S. Weinberg, "Implications of Dynamical Symmetry Breaking," *Phys. Rev. D* **13** (1976) 974–996. [Addendum: Phys.Rev.D 19, 1277–1280 (1979)].

[20] C. T. Hill and E. H. Simmons, "Strong Dynamics and Electroweak Symmetry Breaking," *Phys. Rept.* **381** (2003) 235–402, arXiv:hep-ph/0203079. [Erratum: Phys.Rept. 390, 553–554 (2004)].

[21] C. Csaki, C. Grojean, L. Pilo, and J. Terning, "Towards a realistic model of Higgsless electroweak symmetry breaking," *Phys. Rev. Lett.* **92** (2004) 101802, arXiv:hep-ph/0308038.

[22] M. Saeedhoseini and A. Tofighi, "Strong electroweak phase transition in a model with extended scalar sector," *Adv. High Energy Phys.* **2017** (2017) 7638204, arXiv:1701.02074 [hep-ph].

[23] V. A. Rubakov and D. S. Gorbunov, *Introduction to the Theory of the Early Universe: Hot big bang theory*. World Scientific, Singapore, 2017.

[24] S. R. Coleman and E. J. Weinberg, "Radiative Corrections as the Origin of Spontaneous Symmetry Breaking," *Phys. Rev. D* **7** (1973) 1888–1910.

[25] A. P. Morais and R. Pasechnik, "Probing multi-step electroweak phase transition with multi-peaked primordial gravitational waves spectra," *JCAP* **04** (2020) 036, arXiv:1910.00717 [hep-ph].

[26] C. Caprini *et al.*, "Detecting gravitational waves from cosmological phase transitions with LISA: an update," *JCAP* **03** (2020) 024, arXiv:1910.13125 [astro-ph.CO].

[27] **LISA** Collaboration, P. Amaro-Seoane *et al.*, "Laser Interferometer Space Antenna," arXiv:1702.00786 [astro-ph.IM].

[28] **Particle Data Group** Collaboration, P. Zyla *et al.*, "Review of Particle Physics," *PTEP* **2020** no. 8, (2020) 083C01.

[29] C. Caprini, M. Hindmarsh, S. Huber, T. Konstandin, J. Kozaczuk, G. Nardini, J. M. No, A. Petiteau, P. Schwaller, G. Servant, and D. J. Weir, "Science with the space-based interferometer eLISA. II: gravitational waves from cosmological phase transitions," *Journal of Cosmology and Astroparticle Physics* **2016** no. 04, (Apr, 2016) 001–001. https://doi.org/10.1088/1475-7516/2016/04/001.

[30] M. Hindmarsh, S. J. Huber, K. Rummukainen, and D. J. Weir, "Shape of the acoustic gravitational wave power spectrum from a first order phase transition," *Phys. Rev. D* **96** no. 10, (2017) 103520, arXiv:1704.05871 [astro-ph.CO]. [Erratum: Phys.Rev.D 101, 089902 (2020)].

[31] S. Arrhenius, "Über die dissociationswärme und den einfluss der temperatur auf den dissociationsgrad der elektrolyte," *Zeitschrift für Physikalische Chemie* **4U** no. 1, (1889) 96–116. https://doi.org/10.1515/zpch-1889-0408.

[32] A. D. Linde, "Decay of the False Vacuum at Finite Temperature," *Nucl. Phys. B* **216** (1983) 421. [Erratum: Nucl.Phys.B 223, 544 (1983)].

[33] C. Grojean and G. Servant, "Gravitational Waves from Phase Transitions at the Electroweak Scale and Beyond," *Phys. Rev. D* **75** (2007) 043507, arXiv:hep-ph/0607107.

[34] J. R. Espinosa, T. Konstandin, J. M. No, and G. Servant, "Energy Budget of Cosmological First-order Phase Transitions," *JCAP* **06** (2010) 028, arXiv:1004.4187 [hep-ph].

[35] A. Nicolis, "Relic gravitational waves from colliding bubbles and cosmic turbulence," *Class. Quant. Grav.* **21** (2004) L27, arXiv:gr-qc/0303084.

[36] G. C. Dorsch, S. J. Huber, and T. Konstandin, "Bubble wall velocities in the Standard Model and beyond," *JCAP* **12** (2018) 034, arXiv:1809.04907 [hep-ph].

[37] D. L. C. B. (Oxon.), "Vi. on the rate of explosion in gases," *The London, Edinburgh, and Dublin Philosophical Magazine and Journal of Science* **47** no. 284, (1899) 90–104, https://doi.org/10.1080/14786449908621243. https://doi.org/10.1080/14786449908621243.

[38] Jouguet, "Sur la propagation des réactions chimiques dans les gaz," *Journal de Mathématiques Pures et Appliquées* **1** (1905) 347–425. http://eudml.org/doc/234706.

[39] S. J. Huber and T. Konstandin, "Production of gravitational waves in the nMSSM," *JCAP* **05** (2008) 017, arXiv:0709.2091 [hep-ph].

[40] P. Binetruy, A. Bohe, C. Caprini, and J.-F. Dufaux, "Cosmological Backgrounds of Gravitational Waves and eLISA/NGO: Phase Transitions, Cosmic Strings and Other Sources," *JCAP* **06** (2012) 027, arXiv:1201.0983 [gr-qc].

[41] J. Santiago, "The Physics of Electroweak Symmetry Breaking." http://www.ugr.es/~jsantiago/PoEWSBLectures.pdf.

[42] R. Pasechnik, V. Beylin, V. Kuksa, and G. Vereshkov, "Composite scalar Dark Matter from vector-like $SU(2)$ confinement," *Int. J. Mod. Phys. A* **31** no. 08, (2016) 1650036, arXiv:1407.2392 [hep-ph].

[43] W. R. Inc., "Mathematica, Version 12.3." https://www.wolfram.com/mathematica. Champaign, IL, 2021.

[44] T. Vieu, A. P. Morais, and R. Pasechnik, "Electroweak phase transitions in multi-Higgs models: the case of Trinification-inspired THDSM," *JCAP* **07** (2018) 014, arXiv:1801.02670 [hep-ph].

[45] C. L. Wainwright, "Cosmotransitions: Computing cosmological phase transition temperatures and bubble profiles with multiple fields," *Computer Physics Communications* **183** no. 9, (2012) 2006–2013. https://www.sciencedirect.com/science/article/pii/S0010465512001348.

[46] N. Seto, S. Kawamura, and T. Nakamura, "Possibility of direct measurement of the acceleration of the universe using 0.1-Hz band laser interferometer gravitational wave antenna in space," *Phys. Rev. Lett.* **87** (2001) 221103, arXiv:astro-ph/0108011.

[47] H. Kudoh, A. Taruya, T. Hiramatsu, and Y. Himemoto, "Detecting a gravitational-wave background with next-generation space interferometers," *Phys. Rev. D* **73** (2006) 064006, arXiv:gr-qc/0511145.

[48] S. Kawamura *et al.*, "The Japanese space gravitational wave antenna DECIGO," *Class. Quant. Grav.* **23** (2006) S125–S132.

[49] S. Kuroyanagi, S. Tsujikawa, T. Chiba, and N. Sugiyama, "Implications of the B-mode Polarization Measurement for Direct Detection of Inflationary Gravitational Waves," *Phys. Rev. D* **90** no. 6, (2014) 063513, arXiv:1406.1369 [astro-ph.CO].

[50] J. Crowder and N. J. Cornish, "Beyond LISA: Exploring future gravitational wave missions," *Phys. Rev. D* **72** (2005) 083005, arXiv:gr-qc/0506015.

[51] V. Corbin and N. J. Cornish, "Detecting the cosmic gravitational wave background with the big bang observer," *Class. Quant. Grav.* **23** (2006) 2435–2446, arXiv:gr-qc/0512039.

[52] K. Nakayama and J. Yokoyama, "Gravitational Wave Background and Non-Gaussianity as a Probe of the Curvaton Scenario," *JCAP* **01** (2010) 010, arXiv:0910.0715 [astro-ph.CO].

[53] E. Thrane and J. D. Romano, "Sensitivity curves for searches for gravitational-wave backgrounds," *Phys. Rev. D* **88** no. 12, (2013) 124032, arXiv:1310.5300 [astro-ph.IM].

[54] C. J. Moore, R. H. Cole, and C. P. L. Berry, "Gravitational-wave sensitivity curves," *Class. Quant. Grav.* **32** no. 1, (2015) 015014, arXiv:1408.0740 [gr-qc].

[55] "PTPlot webpage." https://www.ptplot.org/ptplot/.

[56] N. Karnesis, M. Lilley, and A. Petiteau, "Assessing the detectability of a Stochastic Gravitational Wave Background with LISA, using an excess of power approach," *Class. Quant. Grav.* **37** no. 21, (2020) 215017, arXiv:1906.09027 [astro-ph.IM].

[57] C. Caprini, D. G. Figueroa, R. Flauger, G. Nardini, M. Peloso, M. Pieroni, A. Ricciardone, and G. Tasinato, "Reconstructing the spectral shape of a stochastic gravitational wave background with LISA," *JCAP* **11** (2019) 017, arXiv:1906.09244 [astro-ph.CO].

[58] M. B. Hindmarsh, M. Lüben, J. Lumma, and M. Pauly, "Phase transitions in the early universe," arXiv:2008.09136 [astro-ph.CO].